DEVELOPMENTAL DYNAMICS 238:2280–2291, 2009

SPECIAL ISSUE RESEARCH ARTICLE

Transcription Factor GATA-3 Is Essential for Lens Development

Atsuko Maeda,[1] Takashi Moriguchi,[2]* Michito Hamada,[1,5] Manabu Kusakabe,[1] Yuki Fujioka,[1] Takako Nakano,[1] Keigyou Yoh,[3] Kim-Chew Lim,[4] James Douglas Engel,[4] and Satoru Takahashi[1,5]

During vertebrate lens development, the anterior, ectoderm-derived lens vesicle cells differentiate into a monolayer of epithelial cells that retain proliferative potential. Subsequently, they exit the cell cycle and give rise to posterior lens fiber cells that form the lens body. In the present study, we demonstrate that the transcription factor GATA-3 is expressed in the posterior lens fiber cells during embryogenesis, and that GATA-3 deficiency impairs lens development. Interestingly, expression of E-cadherin, a premature lens vesicle marker, is abnormally prolonged in the posterior region of *Gata3* homozygous mutant lenses. Furthermore, expression of γ-crystallin, a differentiation marker for fiber cells, is reduced. This suppressed differentiation is accompanied by an abnormal cellular proliferation, as well as with diminished levels of the cell-cycle inhibitors Cdkn1b/p27 and Cdkn1c/p57 and increased Ccnd2/cyclin D2 abundance. Thus, these observations suggest that GATA-3 is essential for lens cells differentiation and proper cell cycle control. ***Developmental Dynamics 238:2280–2291, 2009.*** **© 2009 Wiley-Liss, Inc.**

Key words: GATA-3; crystallin; lens fiber; differentiation; cell cycle; apoptosis

Accepted 6 June 2009

INTRODUCTION

During vertebrate lens development, a group of head ectoderm cells thickens and forms the lens placode in response to inductive signals from the underlying optic vesicle at embryonic day (e) 9.5 of mouse embryogenesis (Muthukkaruppan, 1965; McAvoy, 1980; Lovicu and McAvoy, 2005; Medina-Martinez and Jamerich, 2007). By e11.5, the lens placode, through invagination, develops into a lens vesicle in which the primary lens fiber cells in the posterior region eventually exit the cell cycle to elongate toward the anterior wall. Three days later, this elongation is complete, and the fully differentiated fiber cells come into contact with the monolayer of cuboidal lens epithelial cells at the anterior of the eye. Throughout most of life, cell proliferation occurs preferentially in a subset of the epithelial cells located near the equatorial zone. After undergoing cell division, they withdraw from the cell cycle and move posteriorly to differentiate into secondary lens fiber cells (McAvoy, 1980; Piatigorsky, 1981; Lovicu and McAvoy, 2005; Medina-Martinez and Jamerich, 2007). As fiber cells differentiate, they rapidly increase in length and volume and accumulate high levels of crystallins, the proteins that account for the transparency and high refractive index of the lens (Piatigorsky, 1981; Lovicu and McAvoy, 2005; Andley, 2007). After completing elongation, fiber cells partially fuse with their neighbors and degrade all membrane bound organelles, including the nuclei.

The cessation of cell proliferation requires the expression of cyclin-dependent kinase (CDK) inhibitors

Additional supporting information may be found in the online version of this article.

[1]Institute of Basic Medical Sciences, University of Tsukuba, Tsukuba, Japan
[2]Department of Medical Biochemistry, Tohoku University Graduate School of Medicine, Sendai, Japan
[3]Institute of Clinical Medicine, University of Tsukuba, Tsukuba, Japan
[4]Department of Cell and Developmental Biology, University of Michigan, Ann Arbor, Michigan
[5]Laboratory Animal Resource Center, University of Tsukuba, Tsukuba, Japan

Grant sponsor: NIH; Grant number: GM28896; Grant sponsor: the Ministry of Education, Culture, Sports, Science and Technology of Japan.

***Correspondence to: Takashi Moriguchi, Tohoku University Graduate School of Medicine, 2-1 Seiryo-cho, Aoba-ku, Sendai 980-8575, Japan. E-mail: moriguch@mail.tains.tohoku.ac.jp**

DOI 10.1002/dvdy.22035
Published online 21 July 2009 in Wiley InterScience (www.interscience.wiley.com).

(CKIs). Two families of CKIs have been identified. The Cip/Kip family contains Cdkn1a/p21, Cdkn1b/p27, and Cdkn1c/p57, which inhibit all kinases involved in the G1/S transition. The INK4a family, composed of Cdkn2b/p15, Cdkn2a/p16, Cdkn2c/p18, and Cdkn2d/p19, specifically inhibit Cdk4 and Cdk6, blocking entry into the cell cycle (Harper and Elledge, 1996; Sherr and Roberts, 1995; Nakayama and Nakayama, 1998). Cdkn1b/p27 and Cdkn1c/p57 are coexpressed during murine lens development, especially in the equatorial zone of the fetal lens (Zhang et al., 1998; Nagahama et al., 2001). The withdrawal of lens fiber cells from the cell cycle largely depends on the expression of Cdkn1b/p27 and Cdkn1c/p57 because in mice that lack these genes, fiber cells continue to proliferate and cause incomplete lens fiber elongation. Eventually, these fiber cells undergo apoptosis in *Cdkn1b/p27*$^{-/-}$ and *Cdkn1c/p57*$^{+/-m}$ (m, denoting maternal active *Cdkn1c/p57* allele) compound mutant mice (Zhang et al., 1998). The other cell cycle regulators involved in lens differentiation are the D-type cyclins. All three D-type cyclins are expressed during lens differentiation, with Ccnd2/Cyclin D2 being the most highly expressed cyclin in the posterior region (Zhang et al., 1998). Down-regulation of Ccnd2/Cyclin D2 in the postmitotic lens fiber cell is required for the maintenance of the postmitotic state (Gomez et al., 1999).

Several genes have been identified that play important roles in the development of the lens. *Gata3* encodes a transcription factor containing two steroid hormone receptor-like zinc fingers that serve as a DNA binding domain, a motif that is highly conserved amongst all six members (GATA-1 to -6) (Patient and McGhee, 2002). These zinc fingers bind most avidly to the consensus motif AGATCTTA (Ko and Engel, 1993). The physiological roles of GATA-3 has been revealed through the analysis of GATA-3–deficient ES cells or various germ line mutant mice: GATA-3 plays a critical role in the differentiation of T lymphocytes, hair follicles, mammary gland, renal, and central nervous systems (Pandolfi et al., 1995; Ting et al., 1996; van Doorninck et al., 1999; Kaufman et al., 2003; Grote et al., 2006; Kouros-Mehr et al., 2006; Kurek et al., 2007; Hasegawa et al., 2007; Asselin-Labat et al., 2007). Moreover, GATA-3 is prominently expressed in the primary sympathetic chain and persists during the development of all sympathoadrenal (SA) lineages, including sympathetic neurons, adrenal chromaffin cells, and para-aortic chromaffin cells (the Zuckerkandl organ; George et al., 1994; Lakshmanan et al., 1999; Lim et al., 2000; Moriguchi et al., 2006).

Gata3 null mutants die around e11 as a consequence of primary noradrenalin biosynthetic defect and secondary cardiac failure (*Gata3*$^{-/-}$; Pandolfi et al., 1995; Lim et al., 2000). But they can be rescued by feeding *Gata3* heterozygous intercrossed dams with synthetic catecholamine intermediates, or by restoring GATA-3 function specifically in SA lineages using the human dopamine β-hydroxylase (hDBH) promoter to direct GATA-3 transgenic expression ($Tg^{hDBH\text{-}G3}$; Lim et al., 2000; Moriguchi et al., 2006). We and others have previously reported that GATA-3 is expressed in lens fiber cells of murine embryos (Oosterwegel et al., 1992; Lakshmanan et al., 1999), although the physiological significance of this observation is unknown. In the present study, we examined the consequences of a GATA-3 loss-of-function mutation in lens development of $Tg^{hDBH\text{-}G3}$-rescued *Gata3* null mutants. We demonstrate that *Gata3* inactivation lead to abnormal development of the posterior lens fiber cells, which exhibit reduced levels of the differentiation marker γ-crystallin, sustained expression of lens vesicle marker E-cadherin and the increased signal of proliferation markers, i.e., BrdU incorporation and Ki67 immunoreactivity. The abnormal proliferation of the lens fiber cells in $Tg^{hDBH\text{-}G3}$-rescued *Gata3* null mutant lenses correlates with reduced levels of Cdkn1b/p27 and Cdkn1c/p57 CKIs as well as increased Ccnd2/Cyclin D2 abundance. Subsequently, these cells succumbed to apoptotic cell death. The molecular pathway that regulates lens differentiation is intimately intertwined with normal cell cycle control, and GATA-3 plays an important role in cellular differentiation of lens fiber cells by inducing cell cycle exit as a part of its regulatory functions.

RESULTS

$Tg^{hDBH\text{-}G3}$-Rescued *Gata3* Null Mutants Displayed Defective Lens Fiber Cell Differentiation

We previously reported that GATA-3 is expressed in lens fiber cells at e12.5, although its ontogeny in the mammalian lens has not been well described (Lakshmanan et al., 1999). To determine the precise temporal and spatial expression profiles of GATA-3 in the lens, we performed GATA-3 immunofluorescence analysis and whole-mount X-gal staining by examining *Gata3lacZ* knock-in heterozygous embryos (van Doorninck et al., 1999). In the developing embryonic lens, *lacZ* expression was first weakly observed at e10.5, then became stronger and was clearly detected in the optic vesicle at e11.5 (Fig. 1A–C). Consistently, GATA-3 immunoreactivity was first specifically observed in the nucleus of e11.5 posterior primary fiber cells (Fig. 1D). By e12.5, when posterior lens fiber cells have normally begun to elongate toward the anterior wall, GATA-3 immunoreactivity was observed in the nucleus of elongating primary lens fiber cells, most prominently in the equatorial zone where fiber cell differentiation first initiates (Fig. 1E,F). GATA-3 immunoreactivity was consistently observed in the fiber cell nuclei along the equatorial zone of e14.5 embryos (Fig. 1G,H), although GATA-3 expression got decreased from e16.5 onward and was hardly observed after birth (data not shown). Importantly, GATA-3 immunoreactivity was observed in differentiated lens fiber cells, but not in proliferating lens epithelial cells of the anterior wall. Hence, GATA-3 expression is strictly confined to the differentiating lens fiber cells of the embryonic eye.

Next, we examined the biological consequences, if any, of *Gata3* loss-of-function mutation on lens development, using $Tg^{hDBH\text{-}G3}$-rescued *Gata3* null mutant mice (Moriguchi et al., 2006). Intriguingly, lenses dissected from e16.5 $Tg^{hDBH\text{-}G3}$-rescued *Gata3* null mutant mice were smaller and

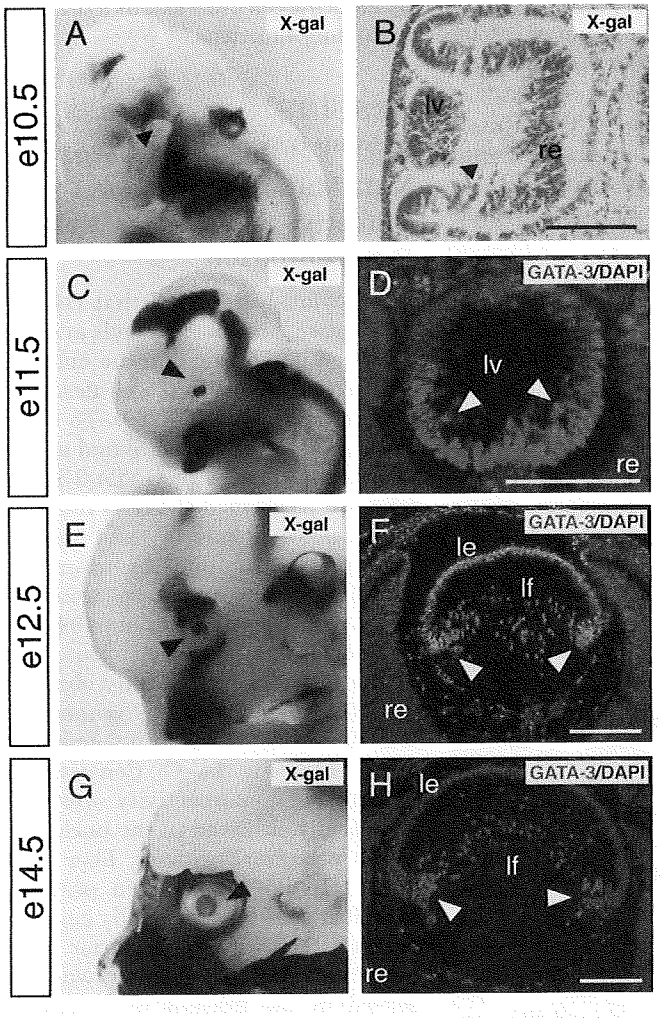

Fig. 1. Optic expression of GATA-3 during embryogenesis. **A–F:** *Gata3lacZ* knock-in heterozygotes at embryonic day (e) 10.5, e11.5, e12.5, and e14.5 were stained with X-gal and photographed in whole-mounts (A,C,E,G) and section (B). Black arrowheads in each panel indicate *lacZ*-positive lens. D,F,H: GATA-3 immunoreactivity was specifically observed in the posterior part of the lens vesicle in e11.5 embryos and in lens fiber cells from e12.5 onward (white arrowheads). le, lens epithelium; lf, lens fiber; lv, lens vesicle; re, retina. Scale bars = 100 μm.

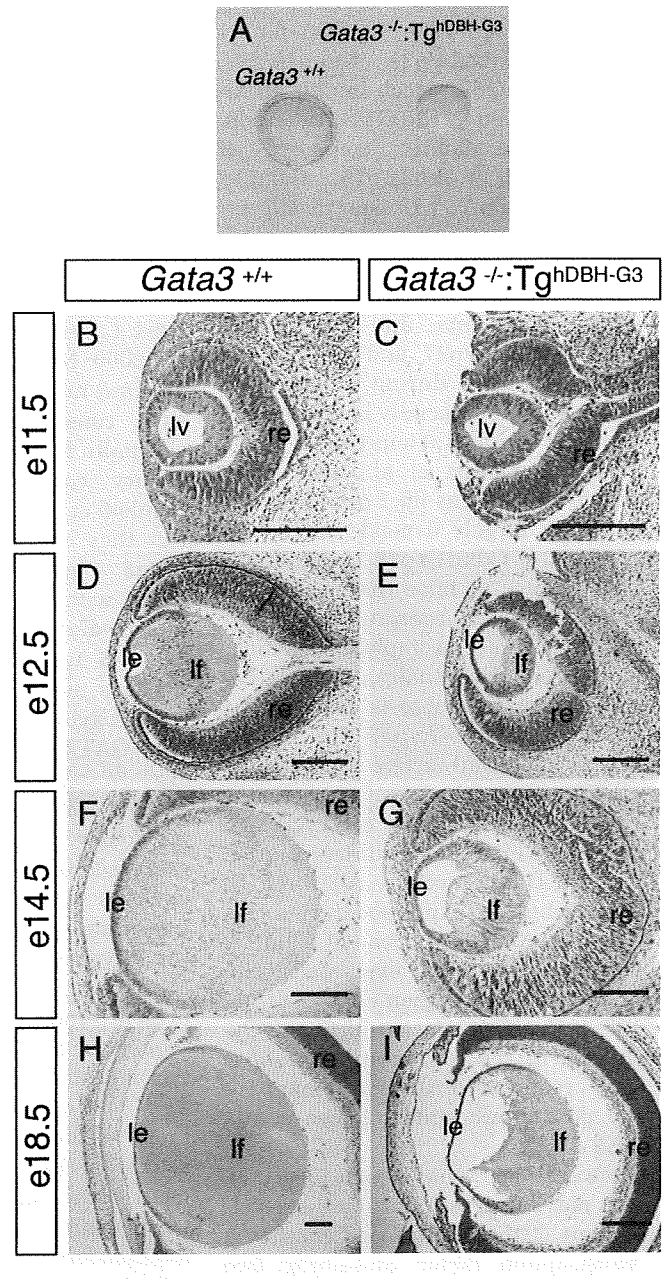

Fig. 2. Defective lens development in rescued *Gata3*$^{-/-}$:Tg$^{hDBH\text{-}G3}$ embryos. **A:** Lenses dissected from embryonic day (e) 16.5 *Gata3*$^{-/-}$:Tg$^{hDBH\text{-}G3}$ embryos are smaller than wild-type. **B–I:** Sagittal sections of e11.5 (B,C), e12.5 (D,E), e14.5 (F,G), and e18.5 (H,I) *Gata3*$^{+/+}$ and *Gata3*$^{-/-}$:Tg$^{hDBH\text{-}G3}$ embryos were stained with hematoxylin and eosin. In e11.5 *Gata3* mutant embryos, the lens vesicle appeared to be normal when compared with wild-type (B,C). From e12.5 onward, GATA-3–deficient lenses were smaller and contained a visible lumen as the lens fiber cells failed to elongate to fill the cavity during late embryogenesis. H,I: Note that the lens fiber cells of e18.5 *Gata3*$^{-/-}$:Tg$^{hDBH\text{-}G3}$ embryos remained highly nucleated (I) in contrast to the wild-type (H) lens fiber cells. lv, lens vesicle, le, lens epithelium; lf, lens fiber; re, retina. Scale bars = 100 μm.

appeared densely opaque when compared with the lenses of wild-type littermates (Fig. 2A). Although the initial formation of the lens vesicle was not affected at e11.5 (Fig. 2B,C), histological analyses of e12.5–e18.5 Tg$^{hDBH\text{-}G3}$-rescued *Gata3* null mutants showed that lens development was disrupted later in development. In the mutants, the lens fiber cells appeared as shortened spindle-shaped cells that failed to extend to the anterior of the lens (Fig. 2E,G). By e18.5, a lumen remained visible in the embryonic eye (Fig. 2E,G, I). And moreover, the degradation of fiber cell nuclei, a marker for terminal differentiation of secondary fiber cells, does not take place in the mutants at E18.5 (Fig. 2H,I). This contrasted starkly with the normal lens development in the control embryo, in which the lumen at e12.5 gradually disappeared by e14.5. By e18.5 the secondary lens fiber cells elongated to fill the cavity and properly degraded their nuclei (Fig. 2D,F,H). In keeping with the spatial expression pattern of GATA-3, the an-

terior epithelial cell layer was essentially unaffected in the $Tg^{hDBH\text{-}G3}$-rescued *Gata3* null mutant lens. Hence, these data indicate that GATA-3 is essential for the differentiation of the lens fiber cells from e12.5 onward.

Crystallin Expression in $Tg^{hDBH\text{-}G3}$-Rescued *Gata3* Null Mutant Lens

The opacity of the GATA-3–deficient lens led us to examine crystallin expression using pan anti–α-, pan anti–β-, or pan anti–γ-crystallin monoclonal antibodies (Sawada et al., 1993). Unexpectedly, the anti-crystallin staining in the *Gata3*-deficient lens hardly differed from that of wild-type lens (Fig. 3A–F). However, DAPI nuclear staining showed that there was increased nuclear density and disorganized alignment of the mutant lens fiber cells (Fig. 3A–F).

We then examined the mRNA level of each crystallin subtype in e16.5 embryonic lenses using quantitative real-time reverse transcriptase polymerase chain reaction assay (qRT-PCR). α-Crystallins are normally expressed in both lens epithelial and fiber cells, whereas members of the β- and γ-crystallin families are expressed more abundantly in the fiber cells (McAvoy, 1978; Murer-Orlando et al., 1987; Goring et al., 1992; Andley, 2007). As anticipated, crystallin mRNA accumulation was moderately to severely reduced in the *Gata3* mutant lenses (Fig. 3G). Of interest, γ-crystallin (γ-A, C, and D) expression, which is most abundantly expressed in fiber cells (Murer-Orlando et al., 1987; Goring et al., 1992; Andley, 2007), was more significantly affected than the other types of crystallins (Fig. 3G). Hence, the presence of GATA-3 activity is essential for normal γ-crystallin expression.

Aberrant Proliferation and Apoptosis in $Tg^{hDBH\text{-}G3}$-rescued *Gata3* Null Mutant Lens

In normal lens development, a precise transition from actively proliferating epithelial cells to terminally differentiating, nonproliferating fiber cells occurs in the equatorial zone of the lens. Our analyses indicated that GATA-3–deficient fiber cells lacked characteristics of fully differentiated lens fiber cells, hence we examined several markers that are indicative of cell proliferation.

E-cadherin is a marker first expressed in lens vesicle cells in early eye development, which then becomes associated with proliferating epithelial cells from e12.5 onward (Wigle et al., 1999; Pontoriero et al., 2009). Although E-cadherin was expressed throughout the entire vesicle of e11.5 wild-type and *Gata3* mutant lens, the expression pattern was different after initiation of fiber cell elongation (Fig 4A,B). At e12.5, E-cadherin expression in wild-type lens was restricted to the lens epithelium, whereas in *Gata3* mutant lens, we observed that the E-cadherin immunoreactivity was still present throughout the lens with stronger staining in the anterior lens epithelium (Fig. 4C,D). The prolonged E-cadherin expression in the posterior lens of e12.5 *Gata3* mutants was quenched 2 days later, as anti-E-cadherin staining was similar in e14.5 wild-type and GATA-3–deficient lenses, although the size of the mutant lens never caught up to wild-type control (Fig. 4E,F). These observations suggest that the GATA-3–deficient posterior lens vesicle cells failed to fully differentiate into fiber cells, so that the posterior half of the lens vesicle retained epithelial cell properties longer than their e12.5 wild-type counterparts.

During later lens development, Ki67- or bromodeoxyuridine (BrdU) -positive proliferating cells were exclusively observed in the epithelial layer of e12.5 and e16.5 wild-type embryos (arrowheads in Fig. 5A,C,E,G). However, e12.5 and e16.5 $Gata3^{-/-}$:$Tg^{hDBH\text{-}G3}$ lenses had a substantially greater number of Ki67- or BrdU-immunopositive nuclei in the posterior fiber cell zone (arrowheads in Fig. 5B,D,F,H,I). Concomitantly, we also detected increased number of programmed cell death in the posterior region of lenses from e12.5 and e16.5 $Gata3^{-/-}$:$Tg^{hDBH\text{-}G3}$ embryos, whereas TUNEL (terminal deoxynucleotidyl transferase-mediated dUTP nick end labeling) -positive nuclei were only rarely detected in the lenses of wild-type control embryos (Fig. 6A–E). This conclusion was further substantiated by the flow cytometric analysis using Annexin-V as an apoptotic cell marker (van Engeland et al., 1998). Lenses from e18.5 $Gata3^{-/-}$:$Tg^{hDBH\text{-}G3}$ or wild-type embryos were dispersed by trypsin treatment, and then single cell suspensions were stained with Annexin-V and 7-Amino Actinomycin D (7-AAD; nucleic acid dye) before being analyzed by flow cytometry. Early apoptotic cells resided in the Annexin-V-single positive fraction, viable cells were negative for both Annexin-V and 7-AAD, and late apoptotic and necrotic cells stained positively for both (Lecoeur et al., 1997; van Engeland et al., 1998; Rasola and Geuna, 2001). As shown in Figure 6F,G, the Annexin-V-single positive fraction (early apoptotic cells) was dramatically increased in the $Gata3^{-/-}$:$Tg^{hDBH\text{-}G3}$ lens (10.85 ± 0.23%; n = 5) in comparison to wild-type lens (3.12 ± 1.23%; n = 5). Late apoptotic and necrotic cells (positive for both 7-AAD and Annexin-V) also significantly increased in the $Gata3^{-/-}$:$Tg^{hDBH\text{-}G3}$ lens (3.09 ± 0.06%; n = 5) compared with the wild-type lens (1.06 ± 0.23%; n = 5; Fig. 6F,G). Hence, the GATA-3–deficient lens fiber cells display epithelial cell property as well as abnormally high proliferative and apoptotic indices.

Elevated Ccnd2/Cyclin D2, Diminished Cdkn1b/p27 and Cdkn1c/p57 Levels in $Gata3^{-/-}$: $Tg^{hDBH\text{-}G3}$ Lens Fiber Cells

Given the abnormal accumulation of proliferative or apoptotic lens fiber cells, we next examined the expression of the cell cycle regulators Cdkn1b/p27, Cdkn1c/p57, and Ccnd2/cyclin D2 in wild-type and $Gata3^{-/-}$:$Tg^{hDBH\text{-}G3}$ lenses. At e12.5, posterior lens vesicle cells begin to express Cdkn1b/p27 and Cdkn1c/p57 in the wild-type lenses (Fig. 7A,E). In e16.5 wild-type embryos, Cdkn1b/p27 and Cdkn1c/p57 were expressed predominantly in the equatorial zone where the epithelial cells exit cell cycle to differentiate into lens fiber cells (Fig. 7C,G). However, both Cdkn1b/p27 and Cdkn1c/p57 expression was conspicuously reduced in e12.5 and e16.5 $Gata3^{-/-}$:$Tg^{hDBH\text{-}G3}$ lenses (Fig. 7B,D,F,H). Meanwhile, anti-Ccnd2/Cyclin D2 labeled nuclei were observed in the equatorial zone of the e16.5 wild-type lens (Fig. 7I), but the fiber cells in the equatorial zone of the e16.5 $Gata3^{-/-}$:$Tg^{hDBH\text{-}G3}$ lens dis-

played significantly more abundant Ccnd2/Cyclin D2 immunoreactivity (Fig. 7J). Indeed, mRNA quantification of isolated e16.5 embryonic lenses demonstrated that both Cdkn1b/p27 and Cdkn1c/p57 mRNA expression was suppressed and that Ccnd2/Cyclin D2 mRNA expression was activated, consistent with the immunohistochemcal observations (Fig. 7K).

Thus, these data indicate that, in the absence of GATA-3, the lens fiber cells exhibited impaired terminal differentiation as evidenced by the abnormal lens morphology, misexpression of epithelial cell characteristics and reduced γ-crystallin levels. Instead, they remained Cdkn1b/p27-negative, Cdkn1c/p57-negative, and Ccnd2/Cyclin D2-positive and failed to properly exit the cell cycle, probably undergoing apoptotic cell death.

Elevated GATA-3 Expression in c-Maf Knock-out Mice

To address possible genetic programs in which GATA-3 might participate during lens development, we examined the expression of several transcription factors that were previously implicated in the regulation of lens development. Prox1 is a homeobox protein that is essential for fiber cell differentiation. Prox1 deficiency in mice leads to aberrant fiber cell proliferation accompanied by suppression of Cdkn1b/p27, Cdkn1c/p57, and γ-crystallins, an alteration in expression that is similar to what is observed in the GATA3-deficient lens (Wigle et al., 1999). Indeed, immunohistochemical analysis of Prox1 demonstrated a quite similar expression pattern in the e14.5 lens to that of GATA-3, except for the epithelial expression (compare Fig. 1F and Fig. 8A). Quantitative RT-PCR performed on GATA-3–deficient e16.5 lenses showed that Prox1 mRNA level was only modestly suppressed in comparison to wild-type controls (Fig. 8C), and Prox1 immunoreactivity was virtually identical in the e14.5 GATA-3-deficient and wild-type lens (Fig. 8A,B). Additionally, we examined the mRNA expression of Sox1, Pax6, and Foxe3, all of which are required for normal lens development and crystalline gene expression. However, the abundance of those transcription factor mRNAs was essentially unchanged in the *Gata3* mutant deficient lens (Hogan et al., 1986; Hill et al., 1991; Matsuo et al., 1993; Nishiguchi et al., 1998; Medina-Martinez et al., 2005; Supp. Fig. S1, which is available online).

c-Maf is a basic leucine zipper transcription factor that is expressed specifically in lens fiber cells of the equatorial zone, and is essential for early lens morphogenesis as well as for crystalline gene activation (Kim et al., 1999; Kawauchi et al., 1999; Ring et al., 2000). c-Maf mRNA levels, as was the case with the previously examined factors, were unchanged in the GATA-3–deficient lens (Fig. S1). However, given the coincident expression pattern of c-Maf and GATA-3 in lens fiber cells, we also examined GATA-3 expression in the c-Maf–deficient embryonic lens, assuming a possible regulatory interaction between those genes in the lens fiber heirarchy. Of interest, we observed an almost eightfold increase of GATA-3 mRNA in c-Maf-deficient e16.5 lens (Fig. 9C). In concert with the elevation in GATA-3 mRNA levels in the c-Maf mutants, increased GATA-3 immunoreactivity was recorded in all vesicle cells of the c-Maf–deficient dysplastic remnant lens at e14.5, demonstrating that GATA-3 expression is either directly or indirectly negatively regulated by c-Maf during normal lens fiber cell development (Fig. 9A,B).

DISCUSSION

In the present study, we demonstrated that GATA-3 expression begins in the developing lens vesicle at mid-embryogenesis (around e11.5) and continues to be expressed in fiber cells throughout embryonic lens development. Its expression is specifically restricted to fiber cells during lens morphogenesis. Consistent with its spatiotemporal expression in the developing lens, the absence of GATA-3 led to interrupted differentiation of posterior lens fiber cells from e12.5 onward, as evidenced by the diminished γ-crystallin levels and prolonged E-cadherin expression in primary lens fiber cells. There was also an increase of mitotic (BrdU- or Ki67-immunopositive) and apoptotic fiber cells in the GATA-3–depleted lens.

Cell Cycle Regulation by GATA Factors Has Been Reported in a Variety of Different Tissues

Recently, it was reported that *Gata2*-deficient mouse embryonic neuroepithelial cells exhibited aberrant proliferation and that GATA-2 overexpression induced neural differentiation by inhibiting the proliferation of neuronal progenitors by means of activation of Cdkn1b/p27 expression (El Wakil et al., 2006). In erythroid cell differentiation, GATA-1 was reported to induce erythromegakaryotic differentiation by suppressing the active cell cycle of hematopoietic progenitor cells by means of induction of Cdkn2a/p16 expression (Pan et al., 2005). Although it is still unclear if GATA-2 or GATA-1 directly regulates Cdkn1b/p27 or Cdkn2a/p16 expression, respectively, these reports as well as the present observations suggest that the potential cell cycle regulatory function for GATA factors in the normal differentiation process acts by activating expression of CKIs. GATA-3

Fig. 3. γ-Crystallin gene expression is reduced in the e16.5 *Gata3*$^{-/-}$:Tg$^{hDBH\text{-}G3}$ lens. **A–F:** Pan anti–α-, β-, and γ-crystallin immunofluorescent staining of sagittal sections from embryonic day (e) 16.5 wild-type and *Gata3* mutant lenses did not reveal any qualitative differences. DAPI (4′,6-diamidine-2-phenylidole-dihydrochloride) nuclear staining showed an increase in nuclear density as well as a disorganized alignment of the mutant lens fiber cells. le, lens epithelium; lf, lens fiber; re, retina. **G:** mRNA levels of each crystallin gene (normalized to Hprt mRNA) in both sides of the lens of individual e16.5 *Gata3*$^{-/-}$:Tg$^{hDBH\text{-}G3}$ (n = 7) and wild-type embryos (n = 6) was assessed by quantitative real-time reverse transcriptase polymerase chain reaction assay (qRT-PCR). Data are presented as mean ± SEM. The statistical significance of differences between *Gata3*$^{+/+}$ and *Gata3*$^{-/-}$:Tg$^{hDBH\text{-}G3}$ are indicated (*$P < 0.05$; Student's *t*-test). Scale bars = 100 μm.

Fig. 4. Prolonged E-cadherin expression in the GATA-3–deficient lens. **A,B:** E-cadherin was expressed throughout the entire vesicle of e11.5 wild-type and *Gata3* mutant lens. **C,E:** E-cadherin expression was restricted to the anterior proliferative epithelium in embryonic day (e) 12.5 and e14.5 wild-type lenses. **D:** In e12.5 *Gata3* mutant lens, an anterioposteriorly graded expression of E-cadherin was observed. **F:** In e14.5 *Gata3* mutant lens, E-cadherin expression pattern was normal. lv, lens vesicle; le, lens epithelium; lf, lens fiber; re, retina. Scale bars = 100 μm.

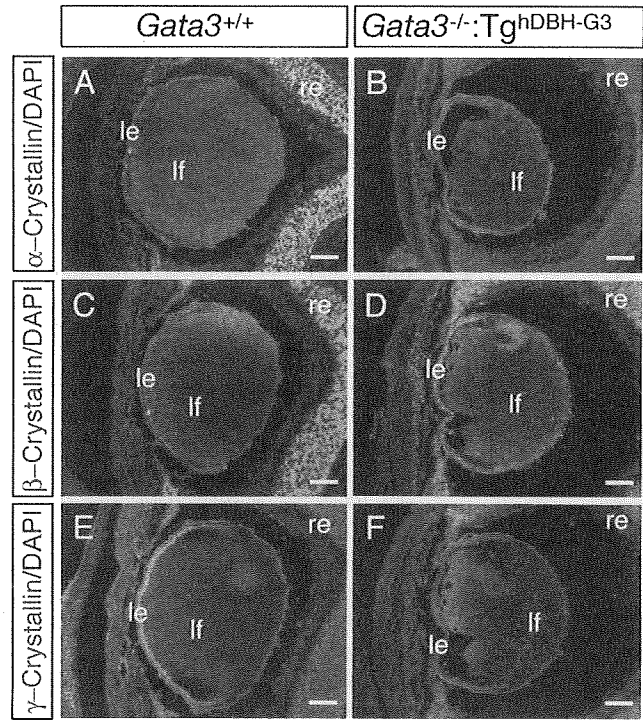

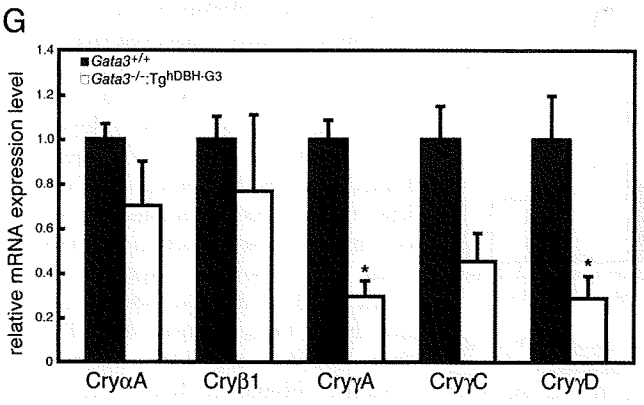

Fig. 3

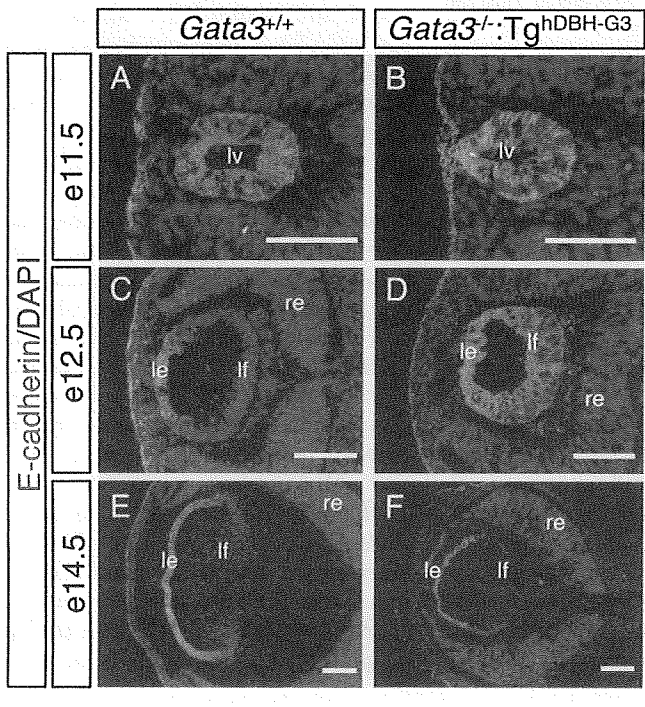

Fig. 4

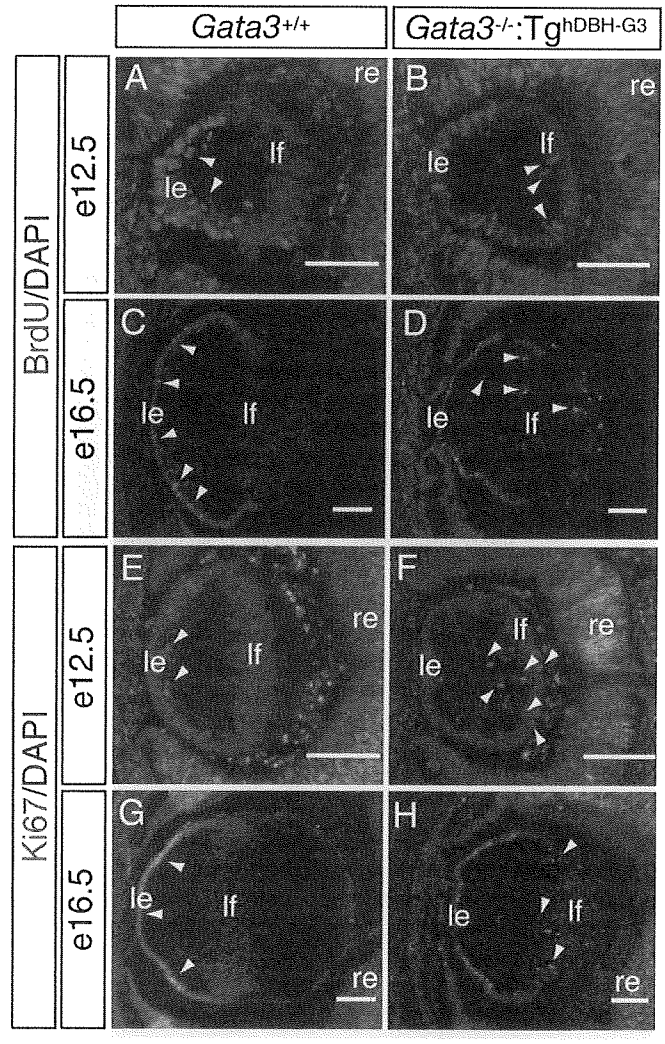

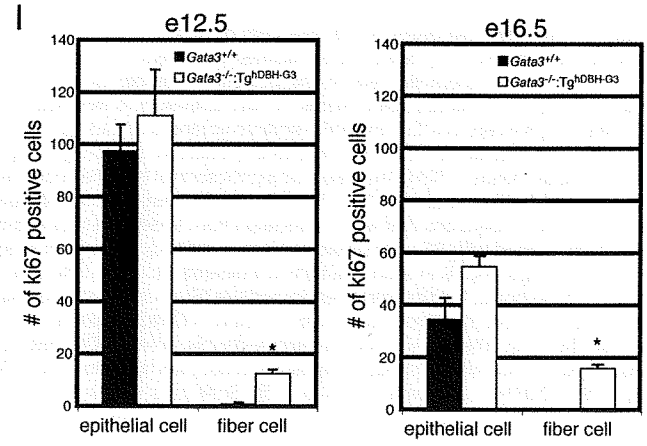

Fig. 5. Altered cellular proliferation in the lenses of *Gata3*$^{-/-}$:Tg$^{hDBH\text{-}G3}$ embryos. **A–H:** In wild-type embryos, Ki67- or bromodeoxyuridine (BrdU) -immunoreactive cells were observed exclusively in the anterior lens epithelium (arrowheads in A,C,E,G), whereas an increased number of mitotic cells were present in the lens fiber cells located in the lens posterior (arrowheads in B,D,F,H) in e12.5 and e16.5 *Gata3*$^{-/-}$:Tg$^{hDBH\text{-}G3}$ embryos. le, lens epithelium; lf, lens fiber; re, retina. **I:** Quantification of ki-67-positive cells in e12.5 and e16.5 embryonic lenses epithelial and fiber cells from wild-type (n = 6) and *Gata3*$^{-/-}$:Tg$^{hDBH\text{-}G3}$ (n = 6) embryos (*$P < 0.05$; Student's *t*-test). Six lenses from six different embryos of each genotype were analyzed. Data are presented as means ± SEM. The statistical significance of the differences between *Gata3*$^{-/-}$:Tg$^{hDBH\text{-}G3}$ and *Gata3*$^{+/+}$ are indicated by (*$P < 0.05$; Student's *t*-test). Scale bars = 100 μm.

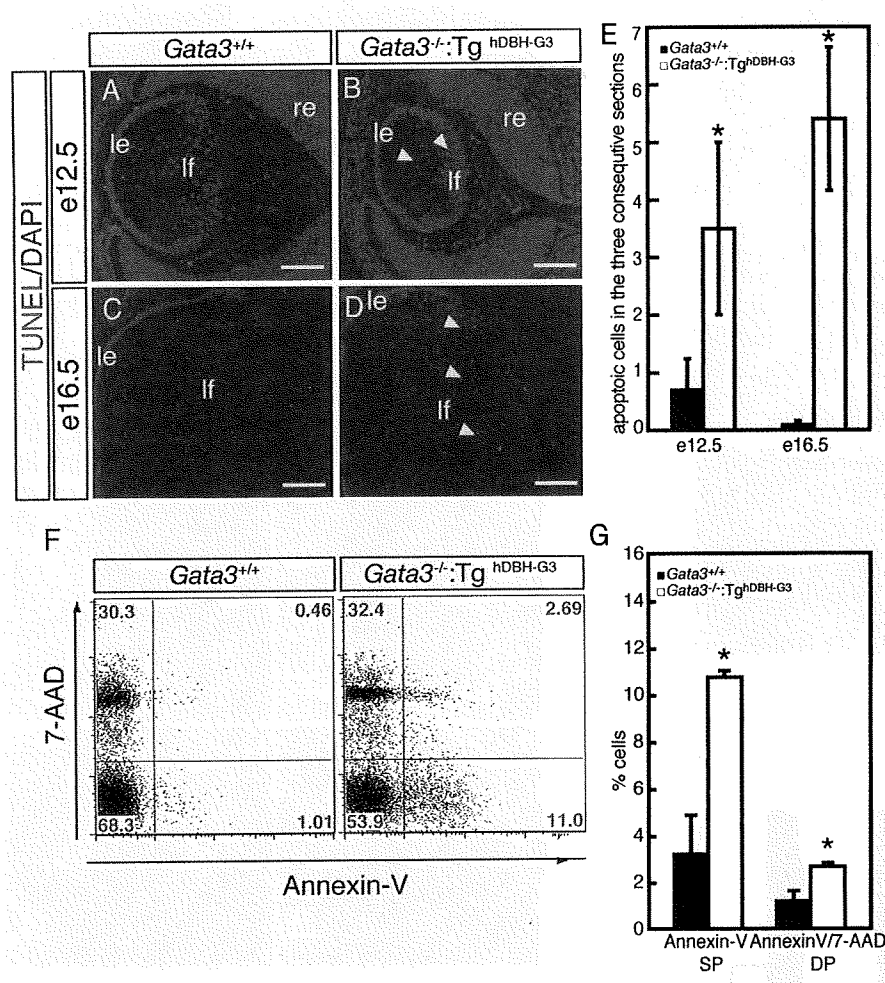

Fig. 6. Increased cell death in lens fiber cells of *Gata3*$^{-/-}$:Tg$^{hDBH\text{-}G3}$ mutant embryos. **A–D:** TUNEL (terminal deoxynucleotidyl transferase-mediated dUTP nick end labeling) assays detected an increase in the number of apoptotic cells in the posterior chamber of embryonic day (e) 12.5 and e16.5 *Gata3*$^{-/-}$:Tg$^{hDBH\text{-}G3}$ lenses (arrowheads). le, lens epithelium; lf, lens fiber; re, retina. **E:** Quantification of TUNEL-positive cells in e12.5 and e16.5 embryonic lenses of wild-type (n = 6) and *Gata3*$^{-/-}$:Tg$^{hDBH\text{-}G3}$ (n = 6) embryos. Six lenses from six different embryos of each genotype were analyzed. Data are presented as means ± SEM. The statistical significance of the differences between *Gata3*$^{-/-}$:Tg$^{hDBH\text{-}G3}$ and *Gata3*$^{+/+}$ are indicated by (*$P < 0.05$; Student's *t*-test). **F:** Representative flow cytometric profiles of single-cell suspensions that were dissociated from lenses of e18.5 wild-type or *Gata3*$^{-/-}$:Tg$^{hDBH\text{-}G3}$ embryos, stained with PE-conjugated Annexin-V antibody (horizontal axis) and 7-AAD (vertical axis). The percentage of cells in each quadrant is indicated. **G:** In the lens fiber cells from e18.5 *Gata3*$^{-/-}$:Tg$^{hDBH\text{-}G3}$ embryos, the Annexin-V-single positive (SP) population, representing early apoptotic cells, increased by more than three-fold (10.85 ± 0.23% in *Gata3* mutant [n = 5], 3.12 ± 1.23% in wild-type control [n = 5]). The 7-AAD- and Annexin-V-double positive (DP) cell population (representing late apoptotic and necrotic cells) also increased by more than two-fold (1.06 ± 0.23% in *Gata3* mutant [n = 5], 3.09 ± 0.06% in wild-type control [n = 5]). Scale bars = 100 μm.

has been reported to suppress abnormal proliferation of mesonephric cells as well as mammary epithelial cells, although the molecular basis for these phenomena remains elusive (Grote et al., 2006; Kouros-Mehr et al., 2006). More recently, transcriptome analysis of GATA-3 conditional deletion in hair follicles indicated that multiple cell cycle regulatory genes were altered in expression (Kurek et al., 2007). Further studies will be necessary to determine how GATA-3 functionally coordinates cell cycle regulation with normal differentiation in a variety of GATA-3–expressing tissues, including lens fiber cells.

Although the mechanistic details of how the loss of GATA-3 results in lens fiber differentiation failure remains to be elucidated, cell cycle regulators may be the potential key molecules underlying the abnormal increase of proliferating cells. In the wild-type lens, the epithelial cells near the equatorial zone exit the cell cycle to give rise to fiber cells, and in the process, they initiate the expression of Cdkn1b/p27 and Cdkn1c/p57. Cdkn1b/p27 and Cdkn1c/p57 cooperatively control the cell cycle exit and the subsequent differentiation of lens fiber cells. Cdkn1b/p27 is normally dispensable for lens development due to its redundancy with Cdkn1c/p57, whereas *Cdkn1b/p27*$^{-/-}$ and *Cdkn1c/p57*$^{+/-m}$, like the *Gata3*-deficient mice, exhibit significant deficiencies in cell cycle withdrawal and in the subsequent differentiation of lens fiber cells (Zhang et al., 1998; Nagahama et al., 2001). In the *Gata3*-deficient lens, we demonstrated that Cdkn1b/p27 and Cdkn1c/p57 immunoreactivities were dramatically suppressed in the equatorial zone, and that their mRNA abundance was reduced in lens, suggesting that GATA-3 deficiency results in the suppression of these two CKIs at the transcription level. However, we have been unable to identify conserved GATA consensus binding sites around the *Cdkn1b/p27* and *Cdkn1c/p57* promoters or to observe GATA-3–dependent *trans*-activation of a reporter gene *cis*-linked to a 1.6-kbp *Cdkn1b/p27* or a 2.0 kbp *Cdkn1c/p57* promoter in several cell lines in co-transfection experiments (data not shown), suggesting that *Cdkn1b/p27* and *Cdkn1c/p57* are either not direct target genes of GATA-3 or that GATA-3 regulates those genes through enhancers that lie outside of the promoter boundaries.

We examined Sox1, Foxe3, Prox1, c-Maf, and Pax6 mRNA expression in e16.5 GATA-3–deficient lenses to examine potential genetic interactions between GATA-3 and each of those other known lens developmental regulators. Sox1 expression initiates in the lens vesicle at around e10 and continues to be expressed in lens fiber cells at e15.5 (Nishiguchi et al., 1998). Foxe3, Prox1, and c-Maf expression is first detected at around e9.0–e9.5 over the lens placode (Wigle et al., 1999; Kawauchi et al., 1999; Medina-Marinez et al., 2005). Foxe3 expression later becomes restricted to the anterior lens epithelium, while Prox1 and c-Maf expression are maintained in the lens fiber cells (Wigle et al., 1999; Kawauchi et al., 1999; Medina-Martinez et al., 2005). Pax6 expression is observed much earlier (in head neural ectoderm) including in the optic pit at e8.0, although from e13.5

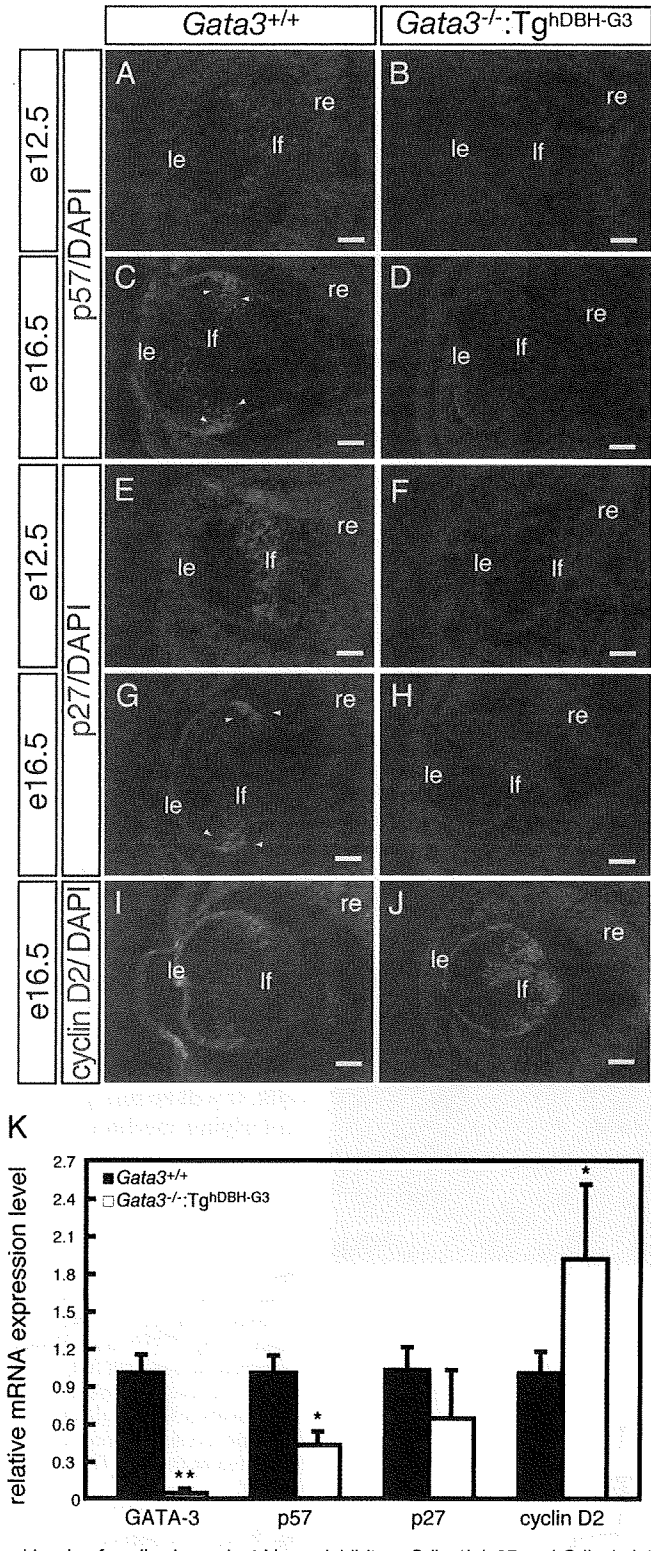

Fig. 7. Altered levels of cyclin-dependent kinase inhibitors Cdkn1b/p27 and Cdkn1c/p57 as well as Ccnd2/Cyclin D2 in *Gata3* mutant lenses. **A,C,E,G:** Strong Cdkn1b/p27 and Cdkn1c/p57 immunoreactive signals were detected in the equatorial zone of e12.5 and e16.5 wild-type lenses (arrowheads). **B,D,F,H:** *Gata3*$^{-/-}$:Tg$^{hDBH\text{-}G3}$ lenses showed significantly diminished intensity of Cdkn1b/p27 and Cdkn1c/p57 labeling. **I,J:** In contrast, *Gata3*$^{-/-}$:Tg$^{hDBH\text{-}G3}$ lens displayed significant induction of Ccnd2/Cyclin D2 expression in comparison to the wild-type control. le, lens epithelium; lf, lens fiber; re, retina. **K:** GATA-3, Cdkn1b/p27, Cdkn1c/p57, and Ccnd2/cyclin D2 mRNA levels (normalized to Hprt mRNA) in whole lenses of individual e16.5 *Gata3*$^{-/-}$:Tg$^{hDBH\text{-}G3}$ (n = 7) and *Gata3*$^{+/+}$ (n = 6) embryos as quantified by quantitative real-time reverse transcriptase polymerase chain reaction assay (qRT-PCR). Data are presented as mean ± SEM. The statistical significance of the differences between *Gata3*$^{-/-}$:Tg$^{hDBH\text{-}G3}$ and *Gata3*$^{+/+}$ are indicated (*$P < 0.05$; **$P < 0.01$; Student's *t*-test). Scale bars = 100 μm.

onward, Pax6 expression is down-regulated in lens fiber cells (Grindley et al., 1995; Donner et al., 2007). Given those spaciotemporal expression patterns and the similarities in lens deficiencies encountered in various mutant mice, we initially expected to establish a genetic regulatory relationship between GATA-3 and Sox1 or Prox1 expression in the developing lens fiber cells. However, all of those transcriptional regulators are in general only modestly, if at all, changed in the GATA-3 deficient lens. Given the later appearance of GATA-3 expression in the e10.5 lens vesicle as well as the relatively mild lens deficiency in *Gata3* mutant mice, we assumed that GATA-3 might be located at a lower position in the hierarchy, but upstream of γ-crystallin and both CKIs (Cdkn1b/p27 and Cdkn1c/p57) in the genetic program of lens development. Of interest, GATA-3 expression is strongly activated in the remnants of the c-Maf–deficient lens. This observation clearly demonstrates that GATA-3 expression is directly or indirectly negatively controlled by c-Maf in normal developing lens fiber cells, so that a c-Maf deficiency derepresses GATA-3 expression, possibly to compensate for the suppressed crystallin gene activation. Precise mapping of lens-specific *Gata3* gene regulatory sequences, which are presumably located within a 2-kbp region lying 5′ to the gene (George et al., 1994; Lieuw et al., 1997), will provide additional insight into the identities of upstream regulators of GATA-3 expression in lens fiber cells.

During differentiation, mature lens fiber cells produce abundant β- and γ-crystallins (McAvoy, 1978). Of the crystalline subtypes, α-crystallins are normally expressed in both lens epithelial and fiber cells, and are first expressed at the lens vesicle stage (McAvoy, 1978; Murer-Orland et al., 1987; Goring et al., 1992; Horwitz, 2003). β-Crystallin expression, which begins at e11 in the mouse embryo, serves as an early marker of fiber cell differentiation, whereas γ-crystallin gene activation initiates around e12.5 (Goring et al., 1992; Nishiguchi et al., 1998; Ring et al., 2000). We showed here that γA, γC and γD-crystallin expression, which are normally restricted in expression to terminally

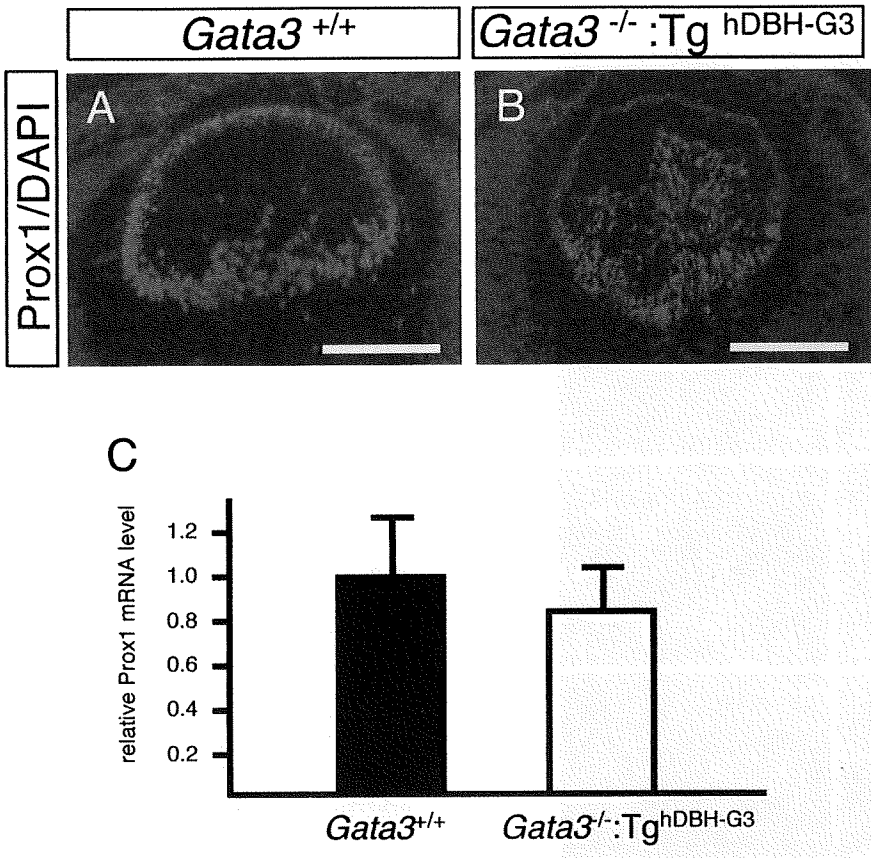

Fig. 8

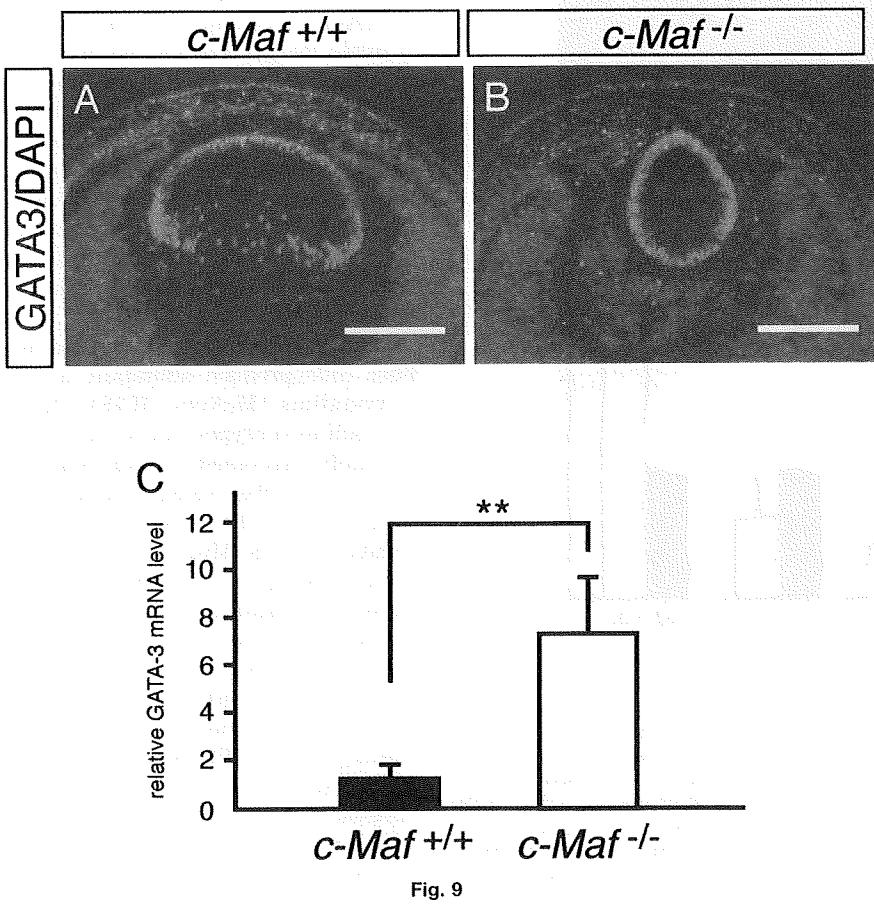

Fig. 9

differentiated fiber cells, were more diminished than αA- and β1-crystallin in *Gata3*$^{-/-}$:Tg$^{hDBH-G3}$ lenses. In the *Gata3* mutant lens, the fiber cell differentiation failure is associated with aberrant accumulation of mitotic posterior cells. There are two possible explanations for this observation. One is that GATA-3 primarily promotes fiber cell differentiation, i.e., activation of γ-*crystallin* genes as well as suppression of E-cadherin expression, so that a GATA-3 deficiency would primarily induce a fiber cell deficiency which in turn would lead to the accumulation of premature epithelial cell-like posterior cells. The other possibility is that the GATA-3 deficiency primarily but indirectly leads to transcriptional suppression of Cdkn1b/p27 and Cdkn1c/p57, which then cause the failure of cell cycle cessation during epithelial to fiber cell transition. Consequently, the posterior lens fiber cells do not fully differentiate and eventually apoptose. Although these two explanations could both be partially correct, cell differentiation and cell cycle cessation are probably tightly interwoven. It will, therefore, be of great interest to further define how GATA-3 functions during induction of cell differentiation as well as how it regulates cell cycle suppression during lens development.

In conclusion, we demonstrated here that GATA-3 is essential for terminal differentiation of lens fiber cells. It will be intriguing to clarify the underlying mechanisms by which the

Fig. 8. Expression of Prox1 in *Gata3* mutant lenses. **A,B:** Prox1 immunoreactivity was approximately equal in embryonic day (e) 16.5 *Gata3*$^{-/-}$:Tg$^{hDBH-G3}$ and *Gata3*$^{+/+}$ littermate embryonic lenses. **C:** e16.5 *Gata3*$^{-/-}$:Tg$^{hDBH-G3}$ (n = 7) embryonic lenses also had statistically equal levels of Prox1 mRNA in comparison with wild-type control embryos (n = 6). Data are presented as mean ± SEM (normalized to Hprt mRNA).

Fig. 9. GATA-3 expression is de-repressed in *c-Maf* mutant lenses. **A,B:** The embryonic day (e) 14.5 c-Maf mutant lenses had significantly greater GATA-3 immunoreactivity than wild-type littermates. **C:** Real-time RT-PCR quantification of GATA-3 mRNA in e16.5 wild-type and c-Maf mutant lenses (normalized to Hprt mRNA). Data are presented as mean ± SEM. The statistical significance of the differences between *c-Maf*$^{+/+}$ (n = 5) and *c-Maf*$^{-/-}$ (n = 6) are indicated (**$P < 0.01$; Student's *t*-test).

TABLE 1. Sequence of Primers Used in Quantitative RT-PCR Analyses and Genotyping

Gene	Sense primer	Antisense primer
hDBH-GATA-3	AGT GAC CAG CTA CAG TCG GA	GGA GAG GGG TCG TTT AAT GG
GATA-3	GGT GGA CGT ACT TTT TAA CAT CGA	CCC TGA CGG AGT TTC CGT AG
Crystallin αA	ACA ACG AGA GGC AGG ATG AC	AGG GGA CAA CCA AGG TGA G
Crystallin β1	AAC TTC CAG GGC AAG AGG AT	AGA TGG GTC GGA AGG ACA T
Crystallin γA	CTC GTG GTA GCG CCT GTA GT	GTC GTG GTA GCG CCT GTA GT
Crystallin γC	TGC TGC CTC ATC CCC CAA CA	TCG CCT AAA AGA GCC AAC TT
Crystallin γD	CTG CTG GAT GCT CTA TGA GC	TTC CGT GAA CTC TAT CAC TTG GC
Cdkn1c/p57	GAG GAC CAG AAC CGC TGG GAC TT	ACT CGC TGT CCA CCT CCA TCC A
Cdkn1b/p27	CGC CAT TAG CGC AAC TGA	CGG CTG CGA AGA TTA GGG
Ccnd1/Cyclin D1	TCT ATC CGG CCC GAG	GAG CTT GTT CAC CAG AAG CAG
Ccnd2/Cyclin D2	ACTGATGTGGATTGTCTCAAAGCCT	CCA CCA GGC ACA ATA GCA ACTACG
Ccnd3/Cyclin D3	GGC TAT GAA CTA CCT GGA TCG CTA	GTA CCT AGA AGC TGC AAT TG
Prox1	GCT CCA ACA TGC TGA AGA CC	TCA TTG ATG GCT TGA CGC GC
Pax6	GGA GAG AAC ACC AAC TCC AT	TCT GGA TAA TGG GTC CTC TC
Foxe3	AGT GGC AGA ACA GCA TCC GC	TCG AGC GTC CAG TAG TTG CC
Sox1	AAG ATG CAC AAC TCG GAG ATC AG	TGT AAT CCG GGT GTT CCT TCA T
c-Maf	CTG CCG CTT CAA GAG GGT GCA GC	TCG CGT GTC ACA CTC ACA TG
HPRT	CAA ACT TTG CTT TCC CTG GT	CAA GGG CAT ATC CAA CAA CA

expression of CKIs and CDKs are controlled by GATA factors, and to identify other cell cycle/apoptosis-related factors which might be responsible for the increased cell death observed in the *Gata3*-deficient lens fiber cells. We conclude, from the data presented here, that the *Gata3* mutant mouse lens may serve as another useful model for elucidating the general principles of cell cycle regulation by GATA transcription factors.

EXPERIMENTAL PROCEDURES

Mice

Generation of c-Maf knock-out mice, *Gata3lacZ* knock-in mice, *Gata3* knock-out mice ($Gata3^{+/-}$), SA lineage-specific GATA-3–expressing transgenic mice ($Tg^{hDBH\text{-}G3}$) and $Gata3^{+/-}$: $Tg^{hDBH\text{-}G3}$ compound heterozygotes were reported previously (Pandolfi et al., 1995; Kawauchi et al., 1999; van Doorninck et al., 1999; Moriguchi et al., 2006). Animals were genotyped by PCR and/or Southern blotting as previously reported (Moriguchi et al., 2006). Primers used to detect the hDBH-GATA-3 transgene are shown in Table 1. All experiments were performed according to the Guide for the Care and Use of Laboratory Animals at the University of Michigan and the University of Tsukuba.

qRT-PCR

Total RNA was extracted from isolated lens tissues of e16.5 wild-type or mutant embryos using TRIZOL (Invitrogen Corp, Carlsbad, CA). First-strand cDNA was synthesized starting with 0.5 μg of total RNA using Superscript III (Invitrogen). qRT-PCR was performed using an ABI PRISM 7700 sequence detector (PE-Applied Biosystems, Foster City, CA) with a 2X SYBR Green PCR master mix (Invitrogen), reverse transcribed cDNA and gene-specific primers as previously described (Moriguchi et al., 2006). The sequences of the primers are listed in Table 1. The data were recorded as means ± standard error of the mean. The statistical significance of differences among means of several groups was determined by Student's *t*-test.

Histological Analysis, Immunofluorescence, and TUNEL Assays

Embryos (e12.5–e18.5) were fixed overnight in 4% paraformaldehyde at 4°C and then processed for paraffin or frozen sections. Paraffin sections (3 μm) were cut with a microtome and processed for either hematoxylin–eosin (HE) staining or immunohistochemistry. The following primary antibodies were used: rabbit anti–GATA-3 (Lim K.-C., unpublished observations), pan anti–α-, β-, and γ-Crystallin monoclonal antibodies (the gifts of K. Kataoka), rabbit anti-Prox1 (Chemicon, CA), rabbit anti–E-cadherin (Takara Biotech, Tokyo, Japan), rabbit anti-Cdkn1b/p27, goat anti-Cdkn1c/p57, and rabbit anti-Ccnd2/Cyclin D2 (all from Santa Cruz Biotechnology, Santa Cruz, CA). For immunofluorescence staining, Alexa Fluor 488-conjugated donkey anti-goat and goat anti-rabbit IgG (Molecular Probes, Eugene, OR) or fluorescein isothiocyanate-conjugated rabbit anti-mouse IgG (Zymed, San Francisco, CA) secondary antibodies were used. Whole-mount X-gal staining was performed as previously described (Lakshmanan et al., 1999).

To analyze 5-bromo-2′-deoxyuridine (BrdU) uptake, pregnant females were administered BrdU (100 μg/gram of body weight) by intraperitoneal injection. After 2 hr, embryos were collected and fixed overnight in 4% PFA. Sections were then stained with mouse anti-BrdU (Becton Dickinson, San Jose, CA). Ki67 is a nuclear protein expressed in all proliferating cells during late G1, S, M, and G2 phases of the cell cycle (Gerdes et al., 1984, 1991). Rabbit anti-Ki67 (Novocastra Laboratories Ltd, UK) was used for detection.

TUNEL assays were performed using the In Situ Apoptosis Detection Kit (Takara BIOTECH) according to

the manufacturer's instructions. For quantification, three transverse sections extending from the center of the lens of each e12.5 or e16.5 embryo were examined by TUNEL or anti-Ki67 antibody (Novocastra Laboratories Ltd, UK). The numbers of TUNEL-positive fiber cells and Ki67-immunoreactive epithelial or fiber cells on the sections was individually determined for each embryo.

Flow Cytometric Analysis of Apoptosis in Lens

Single cell suspension was prepared from e18.5 lens of each mouse genotype by treatment with 0.05% trypsin and 0.53 mM ethylenediaminetetraacetic acid (GIBCO BRL, Gaithersburg, MD) at 37°C for 30 min, and cells were dissociated using fine-tipped pipettes. After the cells were filtered through a 35-μm nylon mesh screen, they were resuspended in phosphate buffered saline containing 4% fluorescence cell sorting. Apoptotic cell analysis was performed using Annexin-V:PE Apoptosis Detection Kit I (BD-Biosciences, San Jose, CA) according to the manufacturer's instructions. Apoptotic cells were stained with Annexin-V, while necrotic cells were distinguished by staining with both Annexin-V and 7-AAD (Herault et al., 1999). FACS analysis was performed with the FACS LSR and CellQuest software (BD-Biosciences).

ACKNOWLEDGMENTS

We thank Drs. S. Kawauchi and J. Maher for critical reading of the manuscript, T. Takeuchi for helpful discussion, and K. Kataoka for providing the anti–α-, β-, and γ-crystallin monoclonal antibodies. We also thank Eriko Naganuma, Naomi Kaneko, and Yuko Suzuki for technical assistance. J.D.E. was funded by the NIH, and S.T. and T.M. were funded by the Ministry of Education, Culture, Sports, Science and Technology of Japan.

REFERENCES

Andley UP. 2007. Crystallins in the eye: function and pathology. Prog Retin Eye Res 26:78–98.

Asselin-Labat ML, Sutherland KD, Barker H, Thomas R, Shackleton M, Forrest NC, Hartley L, Robb L, Grosveld FG, van der Wees J, Lindeman GJ, Visvader JE. 2007. Gata-3 is an essential regulator of mammary-gland morphogenesis and luminal-cell differentiation. Nat Cell Biol 9:201–209.

Donner AL, Ko F, Episkopou V, Maas RL. 2007. Pax6 is misexpressed in Sox1 null lens fiber cells. Gene Expr Patterns 7:606–613.

El Wakil A, Francius C, Wolff A, Pleau-Varet J, Nardelli J. 2006. The GATA2 transcription factor negatively regulates the proliferation of neuronal progenitors. Development 133:2155–2165.

George KM, Leonard MW, Roth ME, Lieuw KH, Kioussis D, Grosveld F, Engel JD. 1994. Embryonic expression and cloning of the murine GATA-3 gene. Development 120:2673–2686.

Gerdes J, Lemke H, Baisch H, Wacker HH, Schwab U, Stein H. 1984. Cell cycle analysis of a cell proliferation-associated human nuclear antigen defined by the monoclonal antibody Ki-67. J Immunol 133:1710–1715.

Gerdes J, Li L, Schlueter C, Duchrow M, Wohlenberg C, Gerlach C, Stahmer I, Kloth S, Brandt E, Flad HD. 1991. Immunobiochemical and molecular biologic characterization of the cell proliferation-associated nuclear antigen that is defined by monoclonal antibody Ki-67. Am J Pathol 38:867–873.

Gomez Lahoz E, Liegeois NJ, Zhang P, Engelman JA, Horner J, Silverman A, Burde R, Roussel MF, Sherr CJ, Elledge SJ, DePinho RA. 1999. Cyclin D- and E-dependent kinases and the p57(KIP2) inhibitor: cooperative interactions in vivo. Mol Cell Biol 19:353–363.

Goring DR, Breitman ML,Tsui LC. 1992. Temporal regulation of six crystallin transcripts during mouse lens development. Exp Eye Res 54:785–795.

Grote D, Souabni A, Busslinger M, Bouchard M. 2006. Pax 2/8-regulated Gata 3 expression is necessary for morphogenesis and guidance of the nephric duct in the developing kidney. Development 133:53–61.

Grindley JC, Davidson DR, Hill RE. 1995. The role of Pax-6 in eye and nasal development. Development 121:1433–1442.

Harper JW, Elledge SJ. 1996. Cdk inhibitors in development and cancer. Curr Opin Genet Dev 6:56–64.

Hasegawa SL, Moriguchi T, Rao A, Kuroha T, Engel JD, Lim KC. 2007. Dosage-dependent rescue of definitive nephrogenesis by a distant Gata3 enhancer. Dev Biol 301:568–577.

Herault O, Colombat P, Domenech J, Degenne M, Bremond JL, Sensebe L, Bernard MC, Binet C. 1999. A rapid single-laser flow cytometric method for discrimination of early apoptotic cells in a heterogenous cell population. Br J Haematol 104:530–537.

Hill RE, Favor J, Hogan BL, Ton CC, Saunders GF, Hanson IM, Prosser J, Jordan T, Hastie ND, van Heyningen V. 1991. Mouse small eye results from mutations in a paired-like homeobox-containing gene. Nature 354:522–525.

Hogan BL, Horsburgh G, Cohen J, Hetherington CM, Fisher G, Lyon MF. 1986. Small eyes (Sey): a homozygous lethal mutation on chromosome 2 which affects the differentiation of both lens and nasal placodes in the mouse. J Embryol Exp Morphol 97:95–110.

Horwitz J. 2003. Alpha-crystallin. Exp Eye Res 76:145–153.

Kaufman CK, Zhou P, Pasolli HA, Rendl M, Bolotin D, Lim KC, Dai X, Alegre ML, Fuchs E. 2003. GATA-3: an unexpected regulator of cell lineage determination in skin. Genes Dev 17:2108–2122.

Kawauchi S, Takahashi S, Nakajima O, Ogino H, Morita M, Nishizawa M, Yasuda K, Yamamoto M. 1999. Regulation of lens fiber cell differentiation by transcription factor c-Maf. J Biol Chem 274: 19254–19260.

Kim JI, Li T, Ho IC, Grusby MJ, Glimcher LH. 1999. Requirement for the c-Maf transcription factor in crystallin gene regulation and lens development. Proc Natl Acad Sci U S A 96:3781–3785.

Ko LJ, Engel JD. 1993. DNA-binding specificities of the GATA transcription factor family. Mol Cell Biol 13:4011–4022.

Kouros-Mehr H, Slorach EM, Sternlicht MD, Werb Z. 2006. GATA-3 maintains the differentiation of the luminal cell fate in the mammary gland. Cell 127: 1041–1055.

Kurek D, Garinis GA, van Doorninck JH, van der Wees J, Grosveld FG. 2007. Transcriptome and phenotypic analysis reveals Gata3-dependent signalling pathways in murine hair follicles. Development 134:261–272.

Lakshmanan G, Lieuw KH, Lim KC, Gu Y, Grosveld F, Engel JD, Karis A. 1999. Localization of distant urogenital system-, central nervous system-, and endocardium-specific transcriptional regulatory elements in the GATA-3 locus. Mol Cell Biol 19:1558–1568.

Lecoeur H, Ledru E, Prevost MC, Gougeon ML. 1997. Strategies for phenotyping apoptotic peripheral human lymphocytes comparing ISNT, annexin-V and 7-AAD cytofluorometric staining methods. J Immunol Methods 209:111–123.

Lieuw KH, Li G, Zhou Y, Grosveld F, Engel JD. 1997. Temporal and spatial control of murine GATA-3 transcription by promoter-proximal regulatory elements. Dev Biol 188:1–16.

Lim KC, Lakshmanan G. Crawford SE, Gu Y, Grosveld F, Engel JD. 2000. Gata3 loss leads to embryonic lethality due to noradrenaline deficiency of the sympathetic nervous system. Nat Genet 25:209–212.

Lovicu FJ, McAvoy JW. 2005. Growth factor regulation of lens development. Dev Biol 280:1–14.

Matsuo T, Osumi-Yamashita N, Noji S, Ohuchi H, Koyama E, Myokai F, Matsuo N, Taniguchi S, Doi H, Iseki S, Ninomiya Y, Fujiwara T, Watanabe T, Eto K. 1993. A mutation in the Pax-6 gene in rat small eye is associated with impaired migration of midbrain crest cells. Nat Genet 3:299–304.

McAvoy JW. 1978. Cell division, cell elongation and distribution of alpha-, beta- and gamma-crystallins in the rat lens. J Embryol Exp Morphol 44:149–165.

McAvoy JW. 1980. Induction of the eye lens. Differentiation 17:137–149.

Medina-Martinez O, Jamerich M. 2007. Foxe view of lens development and disease. Development 134:1455–1463.

Medina-Martinez O, Brownell I, Amaya-Manzanares F, Hu Q, Behringer RR, Jamrich M. 2005. Severe defects in proliferation and differentiation of lens cells in Foxe3 null mice. Mol Cell Biol 25: 8854–8863.

Moriguchi T, Takako N, Hamada M, Maeda A, Fujioka Y, Kuroha T, Huber RE, Hasegawa SL, Rao A, Yamamoto M, Takahashi S, Lim KC, Engel JD. 2006. Gata3 participates in a complex transcriptional feedback network to regulate sympathoadrenal differentiation. Development 133:3871–3881.

Murer-Orlando M, Paterson RC, Lok S, Tsui LC, Breitman ML. 1987. Differential regulation of gamma-crystallin genes during mouse lens development. Dev Biol 119:260–267.

Muthukkaruppan V. 1965. Inductive tissue interaction in the development of the mouse lens in vitro. J Exp Zool 159:269–287.

Nagahama H, Hatakeyama S, Nakayama K, Nagata M, Tomita K, Nakayama K. 2001. Spatial and temporal expression patterns of the cyclin-dependent kinase (CDK) inhibitors p27Kip1 and p57Kip2 during mouse development. Anat Embryol (Berl) 203:77–87.

Nakayama K, Nakayama K. 1998. Cip/Kip cyclin-dependent kinase inhibitors: brakes of the cell cycle engine during development. Bioessays 20:1020–1029.

Nishiguchi S, Wood H, Kondoh H, Lovell-Badge R, Episkopou V. 1998. Sox1 directly regulates the gamma-crystallin genes and is essential for lens development in mice. Genes Dev 12:776–781.

Oosterwegel M, Timmerman J, Leiden J, Clevers H. 1992. Expression of GATA-3 during lymphocyte differentiation and mouse embryogenesis. Dev Immunol 3:1–11.

Pan X, Ohneda O, Ohneda K, Lindeboom F, Iwata F, Shimizu R, Nagano M, Suwabe N, Philipsen S, Lim KC, Engel JD, Yamamoto M. 2005. Graded levels of GATA-1 expression modulate survival, proliferation, and differentiation of erythroid progenitors. J Biol Chem 280:22385–22394.

Pandolfi PP, Roth ME, Karis A, Leonard MW, Dzierzak E, Grosveld FG, Engel JD, Lindenbaum MH. 1995. Targeted disruption of the GATA3 gene causes severe abnormalities in the nervous system and in fetal liver haematopoiesis. Nat Genet 11:40–44.

Patient RK, McGhee JD. 2002. The GATA family (vertebrates and invertebrates). Curr Opin Genet Dev 12:416–422.

Piatigorsky J. 1981. Lens differentiation in vertebrates. A review of cellular and molecular features. Differentiation 19:134–153.

Pontoriero GF, Smith AN, Miller LA, Radice GL, West-Mays JA, Lang RA. 2009. Co-operative roles for E-cadherin and N-cadherin during lens vesicle separation and lens epithelial cell survival. Dev Biol 326:403–417.

Rasola A, Geuna M. 2001. A flow cytometry assay simultaneously detects independent apoptotic parameters. Cytometry 45:151–157.

Ring BZ, Cordes SP, Overbeek PA, Barsh GS. 2000. Regulation of mouse lens fiber cell development and differentiation by the Maf gene. Development 12:307–317.

Sawada K, Agata K, Yoshiki A, Eguchi G. 1993. A set of anti-crystallin monoclonal antibodies for detecting lens specificities: beta-crystallin as a specific marker for detecting lentoidogenesis in cultures of chicken lens epithelial cells. Jpn J Ophthalmol 37:355–368.

Sherr CJ, Roberts JM. 1995. Inhibitors of mammalian G1 cyclin-dependent kinases. Genes Dev 9:1149–1163.

Ting CN, Olson MC, Barton KP, Leiden JM. 1996. Transcription factor GATA-3 is required for development of the T-cell lineage. Nature 384:474–478.

van Doorninck JH, van Der Wees J, Karis A, Goedknegt E, Engel JD, Coesmans M, Rutteman M, Grosveld F, De Zeeuw CI. 1999. GATA-3 is involved in the development of serotonergic neurons in the caudal raphe nuclei. J Neurosci 19:RC12.

van Engeland M, Nieland LJ, Ramaekers FC, Schutte B, Reutelingsperger CP. 1998. Annexin V-affinity assay: a review on an apoptosis detection system based on phosphatidylserine exposure. Cytometry 31:1–9.

Wigle JT, Chowdhury K, Gruss P, Oliver G. 1999. Prox1 function is crucial for mouse lens-fibre elongation. Nat Genet 21:318–322.

Zhang P, Wong C, DePinho RA, Harper JW, Elledge SJ. 1998. Cooperation between the Cdk inhibitors p27(KIP1) and p57(KIP2) in the control of tissue growth and development. Genes Dev 12:3162–3167.

Enhanced humoral immune responses against T-independent antigens in Fcα/μR-deficient mice

Shin-ichiro Honda[a], Naoki Kurita[a], Akitomo Miyamoto[b], Yukiko Cho[a], Kenta Usui[a], Kie Takeshita[a], Satoru Takahashi[c], Teruhito Yasui[d], Hitoshi Kikutani[d], Taroh Kinoshita[e], Teizo Fujita[f], Satoko Tahara-Hanaoka[a], Kazuko Shibuya[a], and Akira Shibuya[a,1]

[a]Department of Immunology and [c]Anatomy and Embryology, Institute of Basic Medical Sciences, Graduate School of Comprehensive Human Sciences, and Center for TARA, University of Tsukuba, 1-1-1 Tennodai, Tsukuba, Ibaraki 305-8575, Japan; [b]Subteam for Manipulation of Cell Fate, Bioresource Center, RIKEN, 3-1-1, Koyadai, Tsukuba, Ibaraki 305-0074, Japan; Departments of [d]Molecular Immunology and [e]Immunoregulation, Research Institute of Microbial Disease, Osaka University, 3-1 Yamadaoka, Suita, Osaka 565-0871, Japan; and [f]Department of Immunology, Fukushima Medical University, 1-Hikarigaoka, Fukushima City, Fukushima 960-1295, Japan

Edited by Toshiyuki Takai, Tohoku University, Sendai, Japan, and accepted by the Editorial Board May 12, 2009 (received for review October 6, 2008)

IgM is an antibody class common to all vertebrates that plays a primary role in host defenses against infection. Binding of IgM with an antigen initiates the complement cascade, accelerating cellular and humoral immune responses. However, the functional role of the Fc receptor for IgM in such immune responses remains obscure. Here we show that mice deficient in Fcα/μR, an Fc receptor for IgM expressed on B cells and follicular dendritic cells (FDCs), have enhanced germinal center formation and affinity maturation and memory induction of IgG3$^+$ B cells after immunization with T-independent (TI) antigens. Moreover, Fcα/μR-deficient mice show prolonged antigen retention by marginal zone B (MZB) cells and FDCs. In vitro studies demonstrate that interaction of the IgM immune complex with Fcα/μR partly suppress TI antigen retention by MZB cells. We further show that downregulation of complement receptor (CR)1 and CR2 or complement deprivation by in vivo injection with anti-CR1/2 antibody or cobra venom factor attenuates antigen retention by MZB cells and germinal center formation after immunization with TI antigens in *Fcα/μR$^{-/-}$* mice. Taken together, these results suggest that Fcα/μR negatively regulates TI antigen retention by MZB cells and FDCs, leading to suppression of humoral immune responses against T-independent antigens.

Fc receptor | IgM | follicular dendritic cells (FDCs) | memory B cells | affinity maturation

IgM is an antibody class common to all vertebrates that constitutes most of the natural antibodies in the pleural and peritoneal cavities of naive hosts (1, 2). In addition, IgM is the first antibody to be produced by naive B cells upon antigen recognition. Therefore, IgM is believed to play an important role in innate immunity against variable bacterial and viral infections (3, 4). Binding of IgM with an antigen initiates the complement cascade, resulting in the acceleration of cellular and humoral immune responses (1). Mice lacking complement 3 or complement 4, or their receptors, complement receptor 1 (CR1) and complement receptor 2 (CR2) (CD35/21), show impaired IgG production in response to T-dependent (TD) antigens (5, 6). Mice lacking the secreted form of IgM (sIgM) also show markedly impaired antibody production and germinal center (GC) formation against TD antigens (7, 8). Thus IgM plays pivotal roles both in innate immunity and in the linkage between innate and adaptive immunity. However, the role of IgM in humoral immune responses against T-independent (TI) antigens is incompletely understood.

During humoral immune responses against TD antigens, an increase in GC size and number is induced in the lymphoid organs; the GC is a principal site for antibody class switching, affinity maturation, and memory B-cell generation (9–11). Follicular dendritic cells (FDCs) play a pivotal role in GC formation by retaining and presenting antigens to follicular B cells (12, 13). In contrast to TD antigens, TI antigens such as polysaccharides and glycolipids of encapsulated bacteria quickly stimulate marginal zone B (MZB) cells in the marginal zone of the follicle to produce IgM and IgG3 class antibodies (14, 15). Although antibody production against TI antigens occurs outside the follicular region, without GC formation (16), several reports have demonstrated that under certain conditions GCs are induced against TI antigens (17, 18). However, the regulation and the immunological consequences of GC formation against TI antigens remain unclear.

We previously identified an Fc receptor for IgM and IgA that we designated Fcα/μR (19, 20). The *Fcα/μR* gene has been mapped to chromosome 1 (1F in mice and 1q32.3 in humans) (19, 21) near several other Fc receptor genes, including *FcγR-I, II, III,* and *IV, FcεRI,* and the *polymeric IgR* (22–24), and Fc receptor homologues (25). Fcα/μR is expressed on the majority of follicular B cells and macrophages but not on granulocytes or T and natural killer cells. Although, unlike other immunoglobulin isotypes, IgM is present in all the vertebrate classes, Fcα/μR is the only receptor for IgM that thus far has been identified on hematopoietic cells of humans and rodents.

We show here that Fcα/μR is expressed preferentially on FDCs and MZB cells, as well as on follicular B cells, in the spleen. Interaction of IgM with Fcα/μR negatively regulates humoral immune responses against TI antigens.

Results

Increased GC Formation in Response to T-Independent Antigen in *Fcα/μR$^{-/-}$* Mice. To investigate the role of Fcα/μR in humoral immune responses in vivo, we established *Fcα/μR*-deficient (*Fcα/μR$^{-/-}$*) mice (see *SI Materials and Methods* and Fig. S1). Because Fcα/μR is expressed on B cells and FDCs (Fig. S2), we examined whether lack of Fcα/μR expression affected B-cell differentiation. Naive *Fcα/μR$^{-/-}$* mice had lymphocyte populations of normal composition in the spleen and showed no differences from their control littermates (*Fcα/μR$^{+/+}$*) in each population of B-cell subsets in the spleen, bone marrow (BM), or peritoneal cavity (data not shown), suggesting that Fcα/μR is not involved in the development of B cells or other lymphocyte lineages. We also observed no differences in the titers of each subclass of IgG and IgM in the sera of naive *Fcα/μR$^{-/-}$* mice (Fig. S3*A*).

Fcα/μR$^{-/-}$ mice demonstrated normal antibody responses

Author contributions: S.-i.H. and A.S. designed research; S.-i.H., N.K., A.M., Y.C., K.U., and K.T. performed research; N.K., S.T., T.Y., H.K., T.K., and T.F. contributed new reagents/analytic tools; S.-i.H., S.T.-H., K.S., and A.S. analyzed data; and A.S. wrote the paper.

The authors declare no conflict of interest.

This article is a PNAS Direct Submission. T.T. is a guest editor invited by the Editorial Board.

Freely available online through the PNAS open access option.

[1]To whom correspondence should be addressed. E-mail: ashibuya@md.tsukuba.ac.jp.

This article contains supporting information online at www.pnas.org/cgi/content/full/0809917106/DCSupplemental.

www.pnas.org/cgi/doi/10.1073/pnas.0809917106

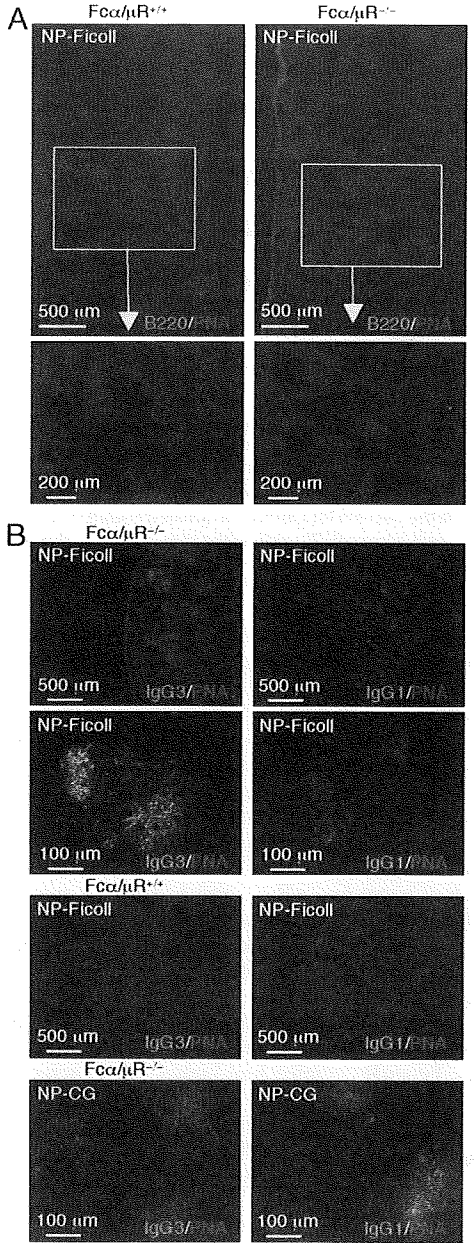

Fig. 1. GC reaction against T-independent (TI) antigens in $Fc\alpha/\mu R^{-/-}$ mice. $Fc\alpha/\mu R^{+/+}$ or $Fc\alpha/\mu R^{-/-}$ mice were immunized i.p. with the TD antigen (NP-CG) emulsified with alum or with the TI antigen NP-Ficoll. A week (for NP-Ficoll) or 2 weeks (for NP-CG) after the immunization, spleen sections were stained with biotinylated PNA, followed by Alexa594-conjugated streptavidin and FITC-conjugated anti-B220 (*A*) or with anti-mouse IgG3 or IgG1 (*B*). Data are representative of 3 independent experiments.

after immunization with the TD antigen 4-hydroxy-3-nitrophenylacetyl-chicken gamma globulin (NP-CG), the TI type 1 antigen NP-LPS, or the TI type 2 antigen NP-Ficoll (Fig. S3*B*). Unexpectedly, however, immunization with either of the TI antigens significantly increased the number and size of GCs in the spleen in $Fc\alpha/\mu R^{-/-}$ mice but not $Fc\alpha/\mu R^{+/+}$ mice (Fig. 1*A* and data not shown). Although these GCs were Bcl-6^{+}, B220^{dull}, and IgD^{low}, similar to those induced after immunization with TD antigens (data not shown), they preferentially produced IgG3 (Fig. 1*B*), rather than the IgG1 detected in the GC B cells induced by the TD antigen NP-CG. Analyses by flow cytometry showed that the numbers of GC B cells, defined as B220^{+}, GL7^{+} cells (26), increased significantly in $Fc\alpha/\mu R^{-/-}$ mice after immunization with the TI antigens NP-Ficoll and NP-LPS but not after immunization with the TD antigen NP-CG (Fig. 2*A* and Table S1). Similar results were obtained by flow cytometry when GC B cells were defined more specifically as PNA^{high}, GL7^{+} cells (Fig. 2*B*). Depletion of CD4^{+} T cells by in vivo injection of an anti-CD4 monoclonal antibody diminished the number of GC B cells after immunization with NP-CG but not after immunization with NP-Ficoll in both $Fc\alpha/\mu R^{-/-}$ and $Fc\alpha/\mu R^{+/+}$ mice (Fig. 2*A*), demonstrating that the increased GC reaction to NP-Ficoll in $Fc\alpha/\mu R^{-/-}$ mice was a T-cell-independent event.

To determine the cell types expressing Fcα/μR responsible for the increased GC formation in response to TI antigens in $Fc\alpha/\mu R^{-/-}$ mice, we established BM chimeric $Fc\alpha/\mu R^{+/+}$ or $Fc\alpha/\mu R^{-/-}$ mice reconstituted with either $Fc\alpha/\mu R^{+/+}$ or $Fc\alpha/\mu R^{-/-}$ BM cells. Because FDCs are radio resistant and therefore are not replaced by donor cells following BM transfer (27), these BM chimeric mice would have donor-derived B cells and recipient-derived FDCs. Immunization with NP-Ficoll increased the number of GC B cells in both $Fc\alpha/\mu R^{+/+}$ and $Fc\alpha/\mu R^{-/-}$ mice reconstituted with $Fc\alpha/\mu R^{-/-}$ and $Fc\alpha/\mu R^{+/+}$ BM cells, respectively, to a significantly greater degree than in $Fc\alpha/\mu R^{+/+}$ mice reconstituted with $Fc\alpha/\mu R^{+/+}$ BM cells (Fig. 2*C*). These results suggest that lack of Fcα/μR expression on both FDCs and B cells is responsible for the enhanced GC formation in response to TI antigens.

Generation of Memory B Cells in Response to TI Antigens in $Fc\alpha/\mu R^{-/-}$ Mice. We then examined whether enhanced GC formation led to memory B-cell generation after immunization with TI antigens in $Fc\alpha/\mu R^{-/-}$ mice. $Fc\alpha/\mu R^{-/-}$ and $Fc\alpha/\mu R^{+/+}$ mice were immunized with NP-Ficoll and were re-challenged with the same antigen 12 weeks after the first immunization. Although the antibody titers again increased in both $Fc\alpha/\mu R^{-/-}$ and $Fc\alpha/\mu R^{+/+}$ mice 1 week after the second immunization, they did not exceed those at 1 week after the first immunization in either group of mice (Fig. S4). These results suggest that memory B cells specific to NP-Ficoll had not been generated. However, it also was possible that the large amount of anti-NP IgG3 that was still detectable in the sera of both groups of mice before the second immunization and that might have been produced by long-lived plasma cells was veiling a small recall response by memory B cells in response to NP-Ficoll.

To dissect further the antibody responses by memory B cells to the second immunization, spleen cells or BM cells from $Fc\alpha/\mu R^{-/-}$ and $Fc\alpha/\mu R^{+/+}$ mice before or 7 weeks after immunization with NP-Ficoll were transferred into SCID mice, which then were challenged with the same antigen on the following day (Fig. 3*A*). A week after the immunization, NP-specific IgG3 production in the SCID mice that had been given the $Fc\alpha/\mu R^{-/-}$ BM cells was significantly greater than that in the SCID mice given the $Fc\alpha/\mu R^{+/+}$ BM cells (Fig. 3*B*). We barely detected NP-specific IgG1 in either group of SCID mice (Fig. 3*B*). In contrast, we did not observe any difference in NP-specific IgG3 production between SCID mice transferred with spleen cells from $Fc\alpha/\mu R^{-/-}$ and $Fc\alpha/\mu R^{+/+}$ mice (data not shown). Because NP-specific IgG3 was not detected in SCID mice that received BM cells from primed mice without the second immunization (Fig. 3*B*), long-lived plasma cells may absent or very rare in BM cells. Collectively, these results suggest that enhanced GC formation in response to TI antigens in $Fc\alpha/\mu R^{-/-}$ mice led to the generation of memory B cells producing IgG3.

Affinity Maturation of IgG3^{+} B Cells Specific to TI Antigens in $Fc\alpha/\mu R^{-/-}$ Mice. We next examined whether increased GC formation also was associated with affinity maturation of B cells in $Fc\alpha/\mu R^{-/-}$ mice. $Fc\alpha/\mu R^{-/-}$ mice and $Fc\alpha/\mu R^{+/+}$ mice were

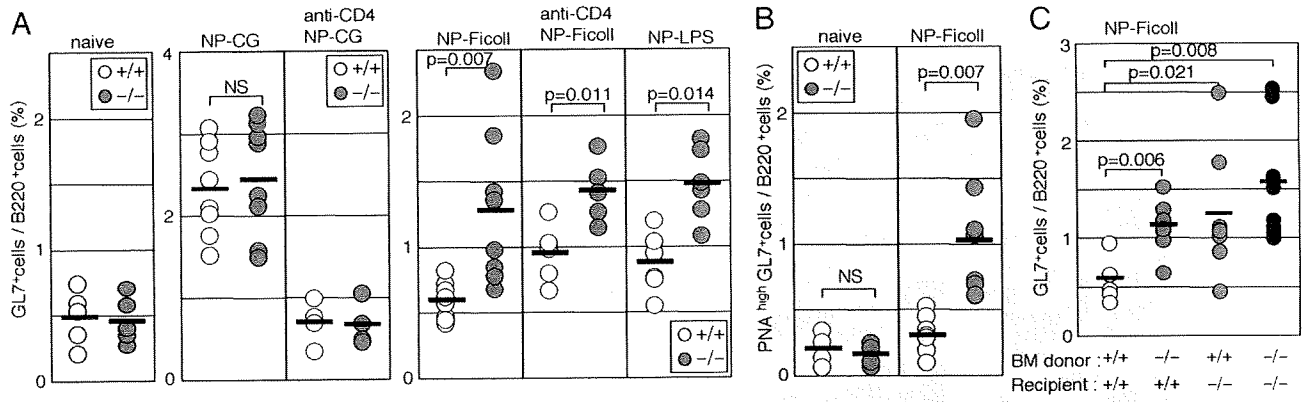

Fig. 2. GC B cells after immunization with T-dependent (TD) or T-independent (TI) antigens in $Fc\alpha/\mu R^{-/-}$ mice. (*A*, *B*) $Fc\alpha/\mu R^{+/+}$ or $Fc\alpha/\mu R^{-/-}$ mice (n = 5–9) were immunized i.p. with TD antigen (NP-CG) emulsified with alum or with TI antigens NP-Ficoll or NP-LPS. A week (for NP-Ficoll and NP-LPS) or 2 weeks (for NP-CG) after the immunization, spleen cells were stained with FITC-conjugated anti-GL-7 and PE-conjugated anti-B220 (*A*) or biotinylated PNA, followed by APC-conjugated streptavidin (*B*). To deplete $CD4^+$ T cells, mice were injected with anti-CD4 (GK1.5) mAb before immunization. Data are representative of 3 independent experiments. (*C*) We injected 5×10^6 BM cells from $Fc\alpha/\mu R^{+/+}$ or $Fc\alpha/\mu R^{-/-}$ mice via the tail vein into lethally irradiated $Fc\alpha/\mu R^{+/+}$ or $Fc\alpha/\mu R^{-/-}$ mice (n = 6–8/group). BM chimeric mice were immunized with NP-Ficoll 6 to 8 weeks later, and $GL7^+$ cells among $B220^+$ cells in the spleen were analyzed 1 week after immunization, as described previously. Data are representative of 2 independent experiments.

immunized with NP-Ficoll or NP-LPS and then were re-challenged with the same antigens 12 weeks later. Sera were collected 1 week and 12 weeks after the first antigen challenges and 1 week after the second antigen challenges and were measured for affinity of NP-specific antibody (Fig. 4*A*). The affinity for NP-specific IgG3 was comparable between $Fc\alpha/\mu R^{-/-}$ and $Fc\alpha/\mu R^{+/+}$ mice 1 week and 12 weeks after the first antigen challenges (data not shown). Although in $Fc\alpha/\mu R^{+/+}$ mice the affinity for NP-specific IgG3 after the second immunization was comparable to that after the first immunization, $Fc\alpha/\mu R^{-/-}$ mice showed significantly higher affinity for NP-specific IgG3 after the second immunization than after the first immunization (Fig. 4*B* and Fig. S5). In contrast, affinities for NP-specific IgG1 were low after the first immunization and were not altered after the second antigen challenge in both $Fc\alpha/\mu R^{-/-}$ and $Fc\alpha/\mu R^{+/+}$ mice (Fig. 4*B* and Fig. S5). These results indicate that $Fc\alpha/\mu R^{-/-}$ mice showed affinity maturation of NP-specific IgG3 after the second challenge with the TI antigens NP-Ficoll or NP-LPS.

To elucidate the molecular basis of the affinity maturation in $Fc\alpha/\mu R^{-/-}$ mice, we examined whether NP-Ficoll induced somatic hypermutation (SHM) in NP-specific $V_H186.2$ $IgG3^+$ B cells in $Fc\alpha/\mu R^{-/-}$ mice. $Fc\alpha/\mu R^{-/-}$ and $Fc\alpha/\mu R^{+/+}$ mice were immunized with NP-Ficoll; then PCR was performed to amplify $V_H186.2$ IgG3 clones from the spleen. We analyzed more than 10 amplified clones and barely detected the $V_H186.2$ clone from the spleen of naive $Fc\alpha/\mu R^{-/-}$ and $Fc\alpha/\mu R^{+/+}$ mice. However, more than half the clones amplified from $Fc\alpha/\mu R^{-/-}$ and $Fc\alpha/\mu R^{+/+}$ mice 1 week after immunization were $V_H186.2$ clones, suggesting that the $V_H186.2$ clone was expanded in response to the immunization. We observed only a few mutations in the $V_H186.2$ clones from $Fc\alpha/\mu R^{-/-}$ and $Fc\alpha/\mu R^{+/+}$ mice 1 week after immunization (Fig. S6). However, in recall responses, $Fc\alpha/\mu R^{-/-}$ mice had higher frequencies of SHM in

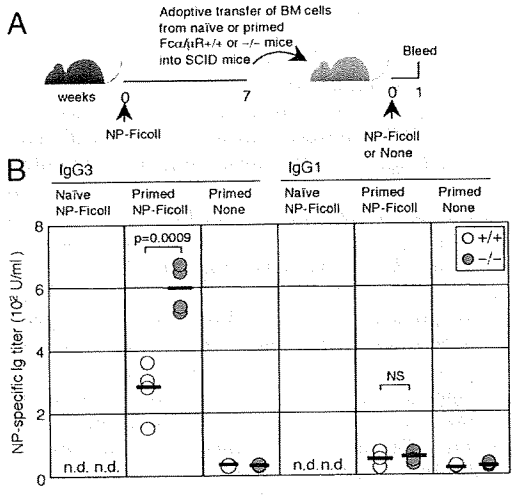

Fig. 3. Recall response against TI antigen in $Fc\alpha/\mu R^{-/-}$ mice. (*A*) $Fc\alpha/\mu R^{+/+}$ or $Fc\alpha/\mu R^{-/-}$ mice were immunized with NP-Ficoll or were not immunized (naive mice). BM cells from naive mice or from the $Fc\alpha/\mu R^{+/+}$ or $Fc\alpha/\mu R^{-/-}$ mice primed with NP-Ficoll were transferred to SCID mice 7 weeks after immunization. The SCID mice then were re-challenged with the same antigen or were not re-challenged. (*B*) Anti-NP IgG3 or IgG1 titers in SCID mice were determined 1 week after the second challenge. n.d., not detected.

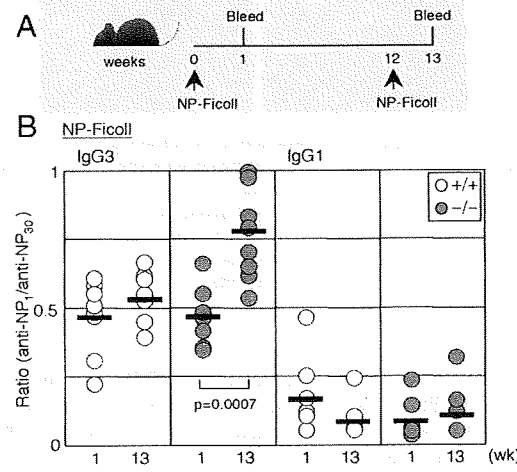

Fig. 4. Affinity maturation after immunization with TI antigen in $Fc\alpha/\mu R^{-/-}$ mice. (*A*) $Fc\alpha/\mu R^{+/+}$ or $Fc\alpha/\mu R^{-/-}$ mice were immunized with NP-Ficoll and were re-challenged with the same antigen 12 weeks later. (*B*) The affinities of anti-NP IgG3 and IgG1 in the sera were determined 1 week after the first immunization and after the second immunization, as described in the experimental procedures.

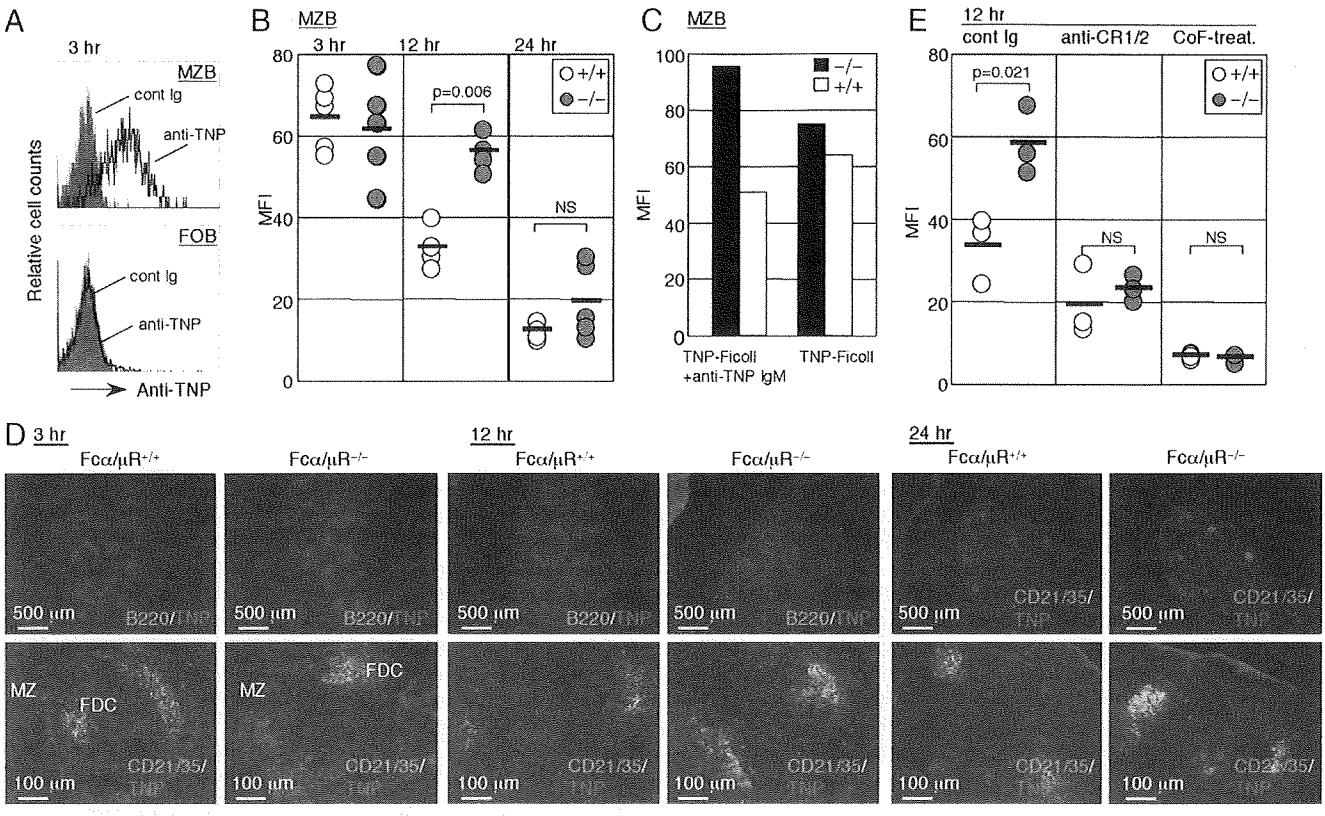

Fig. 5. TI antigen retention on MZB cells and FDCs in $Fc\alpha/\mu R^{-/-}$ mice. (*A*, *B*) $Fc\alpha/\mu R^{+/+}$ or $Fc\alpha/\mu R^{-/-}$ mice were injected i.v. with 50 μg of TNP-Ficoll. Spleen cells were stained with biotin-conjugated anti-TNP, followed by APC-conjugated streptavidin, FITC-conjugated anti-CD21/35, and PE-conjugated anti-CD23 3, 12, or 24 hours after injection. (*A*) Representative flow cytometry profiles of TNP signal on MZB cells ($CD21/35^{high}$, $CD23^-$) and FOB cells ($CD21/35^+$, $CD23^+$) are shown. (*B*) The mean fluorescence intensity (MFI) of the TNP signal on MZB cells is shown. (*C*) Spleen cells from $Fc\alpha/\mu R^{+/+}$ or $Fc\alpha/\mu R^{-/-}$ mice were incubated with TNP-Ficoll alone or with anti-TNP IgM (IgM IC) in the presence of *RAG*-deficient mouse serum. Cells were stained with biotin-conjugated anti-TNP, followed by APC-conjugated streptavidin, FITC-conjugated anti-CD21/35, and PE-conjugated anti-CD23 for flow cytometry analysis. The MFI of TNP signals on MZB- and FOB-gated cells is shown. (*D*) After antigen injection, the spleen sections were stained with biotin-conjugated anti-TNP, followed by Alexa 594-conjugated streptavidin and FITC-conjugated anti-CD21/35 or anti-B220. (*E*) $Fc\alpha/\mu R^{+/+}$ or $Fc\alpha/\mu R^{-/-}$ mice were injected i.v. with anti-CR1/2, control antibody, or CoF before immunization with TNP-Ficoll. Spleen cells were stained with biotin-conjugated anti-TNP 12 hours after the immunization, followed by APC-conjugated streptavidin, FITC-conjugated anti-CD1d, and PE-conjugated anti-CD23. The MFI of TNP signal on MZB-gated cells ($CD1d^{high}$, $CD23^-$) is shown.

the V_H genes of anti-NP IgG3 than did $Fc\alpha/\mu R^{+/+}$ mice (Fig. S6). These increased SHM might cause affinity maturation of NP-specific IgG3 in $Fc\alpha/\mu R^{-/-}$ mice.

Prolongation of TI Antigen Retention on MZB Cells and FDCs in $Fc\alpha/\mu R^{-/-}$ Mice. Our next goal was to determine how Fcα/μR expressed on FDCs and B cells is involved in GC formation. Because MZB cells and FDCs capture antigens efficiently, we speculated that Fcα/μR was involved in TI antigen retention on MZB cells and/or FDCs. To test this hypothesis, we injected 2,4,6-trinitrophenyl (TNP)-Ficoll i.v. into $Fc\alpha/\mu R^{-/-}$ or $Fc\alpha/\mu R^{+/+}$ mice and analyzed antigen retention by using anti-TNP antibody. In both $Fc\alpha/\mu R^{-/-}$ mice and $Fc\alpha/\mu R^{+/+}$ mice, flow cytometry analyses detected the TNP signal on MZB cells ($CD21/35^{high}$, $CD23^-$ cells) but not on follicular B (FOB) cells ($CD21/35^+$, $CD23^+$ cells) 3 hours after TNP-Ficoll injection (Fig. 5*A* and data not shown). The extent of antigen retention on MZB cells, as determined by the intensity of the TNP signals, was comparable in $Fc\alpha/\mu R^{-/-}$ mice and $Fc\alpha/\mu R^{+/+}$ mice 3 hours after antigen injection. Although the TNP signal on MZB cells gradually declined with time, its diminution was much slower in $Fc\alpha/\mu R^{-/-}$ mice than in $Fc\alpha/\mu R^{+/+}$ mice (Fig. 5*B*).

To examine whether IgM is involved in TI antigen retention by MZB cells, we incubated MZB cells derived from $Fc\alpha/\mu R^{-/-}$ mice and $Fc\alpha/\mu R^{+/+}$ mice with either TNP-Ficoll alone or an immune complex (IC) of TNP-Ficoll and anti-TNP IgM in a culture medium containing sera from $RAG^{-/-}$ mice (the medium contained complement but not IgM antibody) and analyzed antigen binding by flow cytometry using anti-TNP antibody. TNP-Ficoll retention (as determined from the mean fluorescence intensity of anti-TNP antibody) by $Fc\alpha/\mu R^{-/-}$ cells and $Fc\alpha/\mu R^{+/+}$ MZB cells in the absence of anti-TNP IgM was comparable, but the $Fc\alpha/\mu R^{-/-}$ MZB cells captured the IgM IC to a greater degree than did the $Fc\alpha/\mu R^{+/+}$ MZB cells (Fig. 5*C*). In contrast, antigen retention was not observed, even in the presence of anti-TNP IgM, on either $Fc\alpha/\mu R^{-/-}$ or $Fc\alpha/\mu R^{+/+}$ FOB cells (data not shown). These results indicated that the interaction of Fcα/μR with IgM IC inhibited TI antigen retention by MZB cells.

Immunohistochemical analyses showed that the antigen was preferentially localized in the marginal zone area 3 hours after antigen injection in both $Fc\alpha/\mu R^{-/-}$ and $Fc\alpha/\mu R^{+/+}$ mice (Fig. 5*D*). Notably, the TNP signal also was detected on FDCs in the follicles in both $Fc\alpha/\mu R^{-/-}$ and $Fc\alpha/\mu R^{+/+}$ mice (Fig. 5*D*), suggesting that TNP-Ficoll is captured by the FDCs as early as 3 hours after antigen injection. Although 12 hours after antigen injection the TNP signal was scarcely detected in the marginal zone area in both $Fc\alpha/\mu R^{-/-}$ and $Fc\alpha/\mu R^{+/+}$ mice and on the FDCs of $Fc\alpha/\mu R^{+/+}$ mice, it still was readily detectable on the FDCs of $Fc\alpha/\mu R^{-/-}$ mice (Fig. 5*D*). These results indicate that the retention of TI antigen on MZB cells and FDCs is prolonged in $Fc\alpha/\mu R^{-/-}$ mice.

Involvement of the Complement Pathway in Humoral Immune Responses against TI Antigens in $Fc\alpha/\mu R^{-/-}$ Mice. Previous reports have demonstrated that humoral immune responses against TI antigens are defective in the absence of complement (28, 29). To determine whether the complement pathway is involved in the increased humoral immune response against TI antigens in $Fc\alpha/\mu R^{-/-}$ mice, we injected $Fc\alpha/\mu R^{-/-}$ and $Fc\alpha/\mu R^{+/+}$ mice with the anti-CR1/2 monoclonal antibody 7G6, which is able to downmodulate the expression of CR1 and CR2 (CD35/21) (30). These mice were injected with the TI antigen TNP-Ficoll 2 days later. Flow cytometric analyses showed that, 12 hours after the antigen injection, antigen retention on the MZB cells of $Fc\alpha/\mu R^{-/-}$ mice had returned to the level in $Fc\alpha/\mu R^{+/+}$ mice (Fig. 5*E*). Because antigen retention by MZB cells is associated with GC formation, we next examined whether the presence of 7G6 antibody also affected GC formation in $Fc\alpha/\mu R^{-/-}$ mice. $Fc\alpha/\mu R^{-/-}$ and $Fc\alpha/\mu R^{+/+}$ mice were immunized with NP-Ficoll 2 days after injection with 7G6 antibody. A week after the immunization, flow cytometric analyses demonstrated that the number of GC B cells in the spleen of $Fc\alpha/\mu R^{-/-}$ mice had returned to the level in $Fc\alpha/\mu R^{+/+}$ mice (Fig. S7*A*). Supporting these results, complement deprivation by injection with cobra venom factor (CoF) attenuated antigen retention and GC formation in response to TI antigens in $Fc\alpha/\mu R^{-/-}$ mice (Fig. 5*E* and Fig. S7*A*). Moreover, the reduction of GC formation by CoF in $Fc\alpha/\mu R^{-/-}$ mice resulted in the diminution of affinity maturation of IgG3 antibody (Fig. S7*B*). Taken together, these results suggest that the increased antigen retention on MZB cells and enhanced GC formation in $Fc\alpha/\mu R^{-/-}$ mice depends on CR1/2.

Discussion

Our results represent the characterization of mice deficient in Fcα/μR. We demonstrated that TI antigens induce enhanced GC formation (Figs. 1 and 2), IgG3 memory response (Fig. 3), and affinity maturation (Fig. 4) in $Fc\alpha/\mu R^{-/-}$ mice. In contrast, we observed no differences between $Fc\alpha/\mu R^{+/+}$ mice and $Fc\alpha/\mu R^{-/-}$ mice in humoral immune response against TD antigens. Although an increase in GC number and size obviously is induced in response to TD antigens (9–11), several lines of evidence have demonstrated that GCs also can be induced against TI antigens, although the response is not as marked as the response to TD antigens (17, 18). However, the structural and functional characteristics of TI antigen-induced GCs have not been elucidated. Although GC reaction was enhanced in $Fc\alpha/\mu R^{-/-}$ mice after immunization with TI antigens, antibody titers in the sera were not elevated, an observation that is in line with previous findings (31). Instead, we observed increased SHM in the V_H genes of IgG3 and affinity maturation of IgG3 against NP-conjugated TI antigens in $Fc\alpha/\mu R^{-/-}$ mice (Fig. S6), consistent with previous reports that SHM occurs within GCs, albeit at low levels, in response to TI antigens (18, 32). We observed increased SHM of anti-NP IgG3 in $Fc\alpha/\mu R^{-/-}$ mice, and this increase might have been associated with affinity maturation of IgG3 after the second challenge by TI antigens. Moreover, we showed that BM cells from $Fc\alpha/\mu R^{-/-}$ mice (but not from $Fc\alpha/\mu R^{+/+}$ mice) primed with TI antigens produced enhanced amounts of anti-NP IgG3 in SCID mice in response to the second antigen challenge (Fig. 3). We indeed detected IgG3, rather than IgG1, localized within enlarged GC areas after immunization with NP-Ficoll (Fig. 1*B*). These results collectively suggest that memory B cells that produced high-affinity IgG3 specific to TI antigens were generated as part of the enhanced GC formation in response to TI antigens in $Fc\alpha/\mu R^{-/-}$ mice.

We also demonstrated prolonged retention of TI antigen on MZB cells and FDCs in $Fc\alpha/\mu R^{-/-}$ mice (Fig. 5). Retention of TI antigens by MZB cells is diminished in complement 3-deficient mice (28, 33), indicating that this process is complement dependent. Here, we found that modulation of complement receptor expression by in vivo injection with anti-CR1/2 antibody or complement deprivation by CoF injection abrogated the TI antigen retention on MZB cells in both $Fc\alpha/\mu R^{-/-}$ and $Fc\alpha/\mu R^{+/+}$ mice (Fig. 5*E*). Moreover, this modulation also diminished the number of GC cells produced in response to TI antigens in $Fc\alpha/\mu R^{-/-}$ mice (Fig. S7*A*). Collectively, these results indicate that increased complement-dependent TI antigen retention on MZB cells leads to enhanced GC reaction in response to TI antigens in $Fc\alpha/\mu R^{-/-}$ mice.

Because the *SLAM* gene, which maps closely to the $Fc\alpha/\mu R$ on chromosome 1, has been shown to affect lymphocyte activity in mice of the 129 strain (34), it is possible that the phenotype observed in the $Fc\alpha/\mu R^{-/-}$ mice might result from the remaining *SLAM* gene derived from E14 ES cells with the 129 genetic background. To address this issue, we subsequently established a new line of $Fc\alpha/\mu R^{-/-}$ mice by using BALB/c ES cells (Fig. S8 *A* and *B*). We also observed increased GC formation and antigen retention on MZB cells and FDCs after TI-antigen challenge in BALB/c Fcα/μR-deficient mice (Fig. S8 *C–F*). Thus, we concluded that the phenotype in the Fcα/μR-deficient mice of B6/129 background resulted from the deficiency of Fcα/μR.

An important question that has remained unanswered is the molecular mechanism of the functional association of the complement cascade with Fcα/μR. Our data suggest that Fcα/μR negatively regulates CR1/2-mediated antigen retention by MZB cells. The classic complement cascade is initiated by C1q binding to the Fc portion of IgM bound to an antigen (35). Therefore, a simple explanation would be that the binding of IgM IC to Fcα/μR prevents C1q from binding to the Fc portion of IgM of the IC, resulting in downregulation of the complement cascade on MZB cells. However, this scenario seemed unlikely, because we did not observe such competition between Fcα/μR and C1q for binding to the Fc portion of IgM in IC (data not shown). Another hypothesis that could explain the Fcα/μR-mediated negative regulation of complement-dependent antigen retention by MZB cells is that Fcα/μR and CR1/2 compete for IgM- or complement-mediated binding of antigen to each receptor. An alternative explanation would be that interaction of IgM IC with Fcα/μR mediates signals that affect CR1/2 function in complement binding. In the present study, we also showed that antigen retention is prolonged on FDCs that markedly express both Fcα/μR and CR1/2 (Fig. 5*D*). Therefore, it also is essential that we clarify whether and how Fcα/μR suppresses CR1/2-mediated antigen retention by FDCs. Further analyses are required to determine the molecular and functional association between Fcα/μR and CR1/2 on MZB cells and FDCs.

We demonstrated that the interaction of IgM with Fcα/μR is primarily involved in antigen retention in vitro (Fig. 5*C*). Therefore, mice deficient in sIgM might be similar to $Fc\alpha/\mu R^{-/-}$ mice. In fact, sIgM-deficient mice show increased IgG2a and IgG2b (7) or IgG3 (8) production in response to NP-Ficoll. We observed increased IgG3 production after the second NP-Ficoll challenge in $Fc\alpha/\mu R^{-/-}$ mice, which demonstrated a phenotype similar to that of sIgM mice in the context of enhanced humoral immune responses against TI antigens. On the other hand, sIgM-deficient mice also show markedly impaired antibody production and GC formation in response to TD antigens (7, 8) that was not observed in $Fc\alpha/\mu R^{-/-}$ mice, suggesting that IgM acts not only as a ligand for Fcα/μR but also has other important roles in the immune response. Of note, mice deficient in sIgM show accelerated development of IgG autoantibodies and autoimmune diseases (36, 37). These results suggest that interaction of the IgM immune complex with Fcα/μR suppresses the humoral immune response against self-antigens. Because most natural antibodies are polyreactive to TI antigens, including a variety of foreign antigens and self-antigens (1, 38), our results shed light on humoral immune responses against both infections and self-antigens.

Materials and Methods

Materials and methods for mice, antibodies, ELISA, immunohistochemistry, generation of BM chimeric mice, and the SHM assay used here are described in *SI Materials and Methods*.

Immunization. For every immunization, wild-type ($Fc\alpha/\mu R^{+/+}$) littermate mice were used as controls for $Fc\alpha/\mu R^{-/-}$ mice. $Fc\alpha/\mu R^{-/-}$ and $Fc\alpha/\mu R^{+/+}$ mice (8 to 12 weeks old) were immunized i.p. with 10 μg NP-CG emulsified with alum as a TD antigen. For TI antigen immunization, 10 μg NP-Ficoll or NP-LPS (Biosearch Technologies) was injected i.p. For recall response, mice were rechallenged with either TI antigen 12 weeks after primary immunization. Sera were collected 1 week after each immunization and were used for ELISA analysis. For in vivo depletion of CD4 T cells, mice were given 100 μg of anti-CD4 (GK1.5) mAb i.p. 2 days before immunization. For downmodulation of CR1/2 in vivo, mice were given 200 μg anti-CR1/2 (7G6) mAb i.p. 2 days before immunization. For complement depletion, 3 μg of CoF was injected into each mouse via the tail vein 1 day before immunization. For the BM cell transfer experiment, 2×10^7 BM cells obtained from $Fc\alpha/\mu R^{-/-}$ or $Fc\alpha/\mu R^{+/+}$ mice 7 weeks after NP-Ficoll immunization were transferred into CB17.SCID mice that were immunized with the same antigen 1 day later.

Affinity Measurement. Antibody affinity was measured by using plates coated with either NP_{30}-BSA or NP_1-BSA. Sera were diluted serially to determine the dilution multitude to the absorbance 2 times greater than background, by using HRP-conjugated goat Abs specific for each mouse immunoglobulin isotype. The ratios of dilution multitudes determined by each plate coated by NP_{30}-BSA or NP_1-BSA were calculated for individual sera.

Antigen Retention Analysis. Mice were injected with 50 μg of TNP-Ficoll (Biosearch) via the tail vein. The splenocytes then were stained with biotin-conjugated hamster anti-TNP IgG, followed by allophycocyanin (APC)-conjugated streptavidin in combination with FITC-conjugated anti-CD21/35 and phycoerythrin (PE)-conjugated anti-CD23 (PharMingen) for flow cytometric analyses. For immunohistochemical analyses, frozen sections of the spleen were incubated with biotin-conjugated hamster anti-TNP IgG (PharMingen), followed by Alexa 594-conjugated streptavidin (Invitrogen) in combination with FITC-conjugated anti-CD21/35 or anti-B220. For the in vitro experiment, TNP-Ficoll was incubated with anti-TNP mouse IgM (PharMingen) for 30 min at 37 °C and then cultured for 15 min at 37 °C with splenocytes in 1% $RAG^{-/-}$ mouse-derived serum containing TC buffer [140 mM NaCl, 2 mM $CaCl_2$, 2 mM $MgCl_2$, 10 mM Tris (pH 7.5), supplemented with 1% BSA]. The cells were stained for flow cytometric analysis as described earlier in the article.

Statistics. Statistical analyses were performed by using Student's unpaired *t* test.

ACKNOWLEDGMENTS. We thank L. Lanier and J. Cyster for critical reading of this manuscript and Y. Soeda for secretarial assistance. This research was supported in part by grants provided by the Ministry of Education, Science, and Culture of Japan; Special Coordination Funds from the Science and Technology Agency of the Japanese Government; the Program for Promotion of Fundamental Studies in Health Science of the National Institute of Biomedical Innovation (NIBIO); and the Uehara Memorial Foundation.

1. Ochsenbein AF, Zinkernagel RM (2000) Natural antibodies and complement link innate and acquired immunity. *Immunol Today* 21(12):624–630.
2. Casali P, Schettino EW (1996) Structure and function of natural antibodies. *Curr Top Microbiol Immunol* 210:167–179.
3. Ochsenbein AF, et al. (1999) Control of early viral and bacterial distribution and disease by natural antibodies. *Science* 286(5447):2156–2159.
4. Boes M, Prodeus AP, Schmidt T, Carroll MC, Chen J (1998) A critical role of natural immunoglobulin M in immediate defense against systemic bacterial infection. *J Exp Med* 188(12):2381–2386.
5. Carroll MC (2004) The complement system in regulation of adaptive immunity. *Nat Immunol* 5(10):981–986.
6. Fischer MB, et al. (1996) Regulation of the B cell response to T-dependent antigens by classical pathway complement. *J Immunol* 157(2):549–556.
7. Boes M, et al. (1998) Enhanced B-1 cell development, but impaired IgG antibody responses in mice deficient in secreted IgM. *J Immunol* 160(10):4776–4787.
8. Ehrenstein MR, O'Keefe TL, Davies SL, Neuberger MS (1998) Targeted gene disruption reveals a role for natural secretory IgM in the maturation of the primary immune response. *Proc Natl Acad Sci USA* 95(17):10089–10093.
9. Kelsoe G (1996) Life and death in germinal centers (redux). *Immunity* 4(2):107–111.
10. MacLennan IC (2005) Germinal centers still hold secrets. *Immunity* 22(6):656–657.
11. Manser T (2004) Textbook germinal centers? *J Immunol* 172(6):3369–3375.
12. Park CS, Choi YS (2005) How do follicular dendritic cells interact intimately with B cells in the germinal centre? *Immunology* 114(1):2–10.
13. Chaplin DD, Zindl CL (2006) Taking control of follicular dendritic cells. *Immunity* 24(1):13–15.
14. Martin F, Kearney JF (2002) Marginal-zone B cells. *Nature Reviews Immunology* 2(5):323–335.
15. Lopes-Carvalho T, Kearney JF (2004) Development and selection of marginal zone B cells. *Immunol Rev* 197:192–205.
16. MacLennan IC, et al. (2003) Extrafollicular antibody responses. *Immunol Rev* 194:8–18.
17. de Vinuesa CG, et al. (2000) Germinal centers without T cells. *J Exp Med* 191(3):485–494.
18. Lentz VM, Manser T (2001) Cutting edge: Germinal centers can be induced in the absence of T cells. *J Immunol* 167(1):15–20.
19. Shibuya A, et al. (2000) Fc alpha/mu receptor mediates endocytosis of IgM-coated microbes. *Nat Immunol* 1(5):441–446.
20. Sakamoto N, et al. (2001) A novel Fc receptor for IgA and IgM is expressed on both hematopoietic and non-hematopoietic tissues. *Eur J Immunol* 31(5):1310–1316.
21. Shimizu Y, et al. (2001) Fc(alpha)/mu receptor is a single gene-family member closely related to polymeric immunoglobulin receptor encoded on chromosome 1. *Immunogenetics* 53(8):709–711.
22. Daeron M (1997) Fc receptor biology. *Annu Rev Immunol* 15:203–234.
23. Ravetch JV, Bolland S (2001) IgG Fc receptors. *Annu Rev Immunol* 19:275–290.
24. Nimmerjahn F, Ravetch JV (2006) Fcgamma receptors: Old friends and new family members. *Immunity* 24(1):19–28.
25. Davis RS, Wang YH, Kubagawa H, Cooper MD (2001) Identification of a family of Fc receptor homologs with preferential B cell expression. *Proc Natl Acad Sci USA* 98(17):9772–9777.
26. Takahashi Y, Dutta PR, Cerasoli DM, Kelsoe G (1998) In situ studies of the primary immune response to (4-hydroxy-3-nitrophenyl)acetyl. V. Affinity maturation develops in two stages of clonal selection. *J Exp Med* 187(6):885–895.
27. Ahearn JM, et al. (1996) Disruption of the Cr2 locus results in a reduction in B-1a cells and in an impaired B cell response to T-dependent antigen. *Immunity* 4(3):251–262.
28. Guinamard R, Okigaki M, Schlessinger J, Ravetch JV (2000) Absence of marginal zone B cells in Pyk-2-deficient mice defines their role in the humoral response. *Nat Immunol* 1(1):31–36.
29. Fearon DT, Carroll MC (2000) Regulation of B lymphocyte responses to foreign and self-antigens by the CD19/CD21 complex. *Annu Rev Immunol* 18:393–422.
30. Thyphronitis G, et al. (1991) Modulation of mouse complement receptors 1 and 2 suppresses antibody responses in vivo. *J Immunol* 147(1):224–230.
31. Garcia de Vinuesa C, O'Leary P, Sze DM, Toellner KM, MacLennan IC (1999) T-independent type 2 antigens induce B cell proliferation in multiple splenic sites, but exponential growth is confined to extrafollicular foci. *Eur J Immunol* 29(4):1314–1323.
32. Toellner KM, et al. (2002) Low-level hypermutation in T cell-independent germinal centers compared with high mutation rates associated with T cell-dependent germinal centers. *J Exp Med* 195(3):383–389.
33. Lopes-Carvalho T, Foote J, Kearney JF (2005) Marginal zone B cells in lymphocyte activation and regulation. *Curr Opin Immunol* 17(3):244–250.
34. Kumar KR, et al. (2006) Regulation of B cell tolerance by the lupus susceptibility gene Ly108. *Science* 312(5780):1665–1669.
35. Roozendaal R, Carroll MC (2006) Emerging patterns in complement-mediated pathogen recognition. *Cell* 125(1):29–32.
36. Boes M, et al. (2000) Accelerated development of IgG autoantibodies and autoimmune disease in the absence of secreted IgM. *Proc Natl Acad Sci USA* 97(3):1184–1189.
37. Ehrenstein MR, Cook HT, Neuberger MS (2000) Deficiency in serum immunoglobulin (Ig)M predisposes to development of IgG autoantibodies. *J Exp Med* 191(7):1253–1258.
38. Binder CJ, Silverman GJ (2005) Natural antibodies and the autoimmunity of atherosclerosis. *Springer Seminars in Immunopathology* 26(4):385–404.

Vol 463|28 January 2010|doi:10.1038/nature08636

LETTERS

Innate production of T_H2 cytokines by adipose tissue-associated c-Kit$^+$Sca-1$^+$ lymphoid cells

Kazuyo Moro[1,4], Taketo Yamada[2], Masanobu Tanabe[3], Tsutomu Takeuchi[3], Tomokatsu Ikawa[5], Hiroshi Kawamoto[5], Jun-ichi Furusawa[1], Masashi Ohtani[1,6], Hideki Fujii[1] & Shigeo Koyasu[1,7]

Innate immune responses are important in combating various microbes during the early phases of infection. Natural killer (NK) cells are innate lymphocytes that, unlike T and B lymphocytes, do not express antigen receptors but rapidly exhibit cytotoxic activities against virus-infected cells and produce various cytokines[1,2]. Here we report a new type of innate lymphocyte present in a novel lymphoid structure associated with adipose tissues in the peritoneal cavity. These cells do not express lineage (Lin) markers but do express c-Kit, Sca-1 (also known as Ly6a), IL7R and IL33R. Similar lymphoid clusters were found in both human and mouse mesentery and we term this tissue 'FALC' (fat-associated lymphoid cluster). FALC Lin$^-$c-Kit$^+$Sca-1$^+$ cells are distinct from lymphoid progenitors[3] and lymphoid tissue inducer cells[4]. These cells proliferate in response to IL2 and produce large amounts of T_H2 cytokines such as IL5, IL6 and IL13. IL5 and IL6 regulate B-cell antibody production and self-renewal of B1 cells[5–7]. Indeed, FALC Lin$^-$c-Kit$^+$Sca-1$^+$ cells support the self-renewal of B1 cells and enhance IgA production. IL5 and IL13 mediate allergic inflammation and protection against helminth infection[8,9]. After helminth infection and in response to IL33, FALC Lin$^-$c-Kit$^+$Sca-1$^+$ cells produce large amounts of IL13, which leads to goblet cell hyperplasia—a critical step for helminth expulsion. In mice devoid of FALC Lin$^-$c-Kit$^+$Sca-1$^+$ cells, such goblet cell hyperplasia was not induced. Thus, FALC Lin$^-$c-Kit$^+$Sca-1$^+$ cells are T_H2-type innate lymphocytes, and we propose that these cells be called 'natural helper cells'.

The cytokine receptor common γ chain (γ_c) is critical for the differentiation of lymphocytes as well as lymphoid tissue inducer (LTi) cells. The latter have an essential role in the development of lymphoid tissues such as lymph nodes, Peyer's patches and isolated lymphoid follicles[10,11]. Herein we identified a previously unrecognized γ_c-dependent lymphoid structure in mouse. Clusters of lymphocytes were observed along the blood vessels in the mouse mesentery—an adipose tissue in the peritoneal cavity (Fig. 1a, b). These clusters were surrounded by adipose tissues (Fig. 1c), and 5–50 clusters were found throughout the mesentery. The size of each cluster was 100–500 μm in diameter, and the number and size of clusters increased with age. Although lymphocytes were the dominant cell population in the cluster, unlike lymph nodes, no fibrous capsule was present around the clusters, and lymphocytes were in direct contact with ambient adipocytes (Supplementary Fig. 1a). The blood capillaries in these clusters were filled with lymphocytes and a few red blood cells (Supplementary Fig. 1b).

Flow cytometric analysis (Fig. 1d) identified a cell population expressing c-Kit and Sca-1 but no Lin markers (CD3ε, CD4, CD8α, TCRβ, TCRδ, CD5, CD19, B220 (encoded by *Ptprc*), NK1.1 (Klrb1c), Ter119 (Ly76), Gr-1 (Ly6g), Mac-1 (Itgam), CD11c (Itgax) and FcεRIα) that

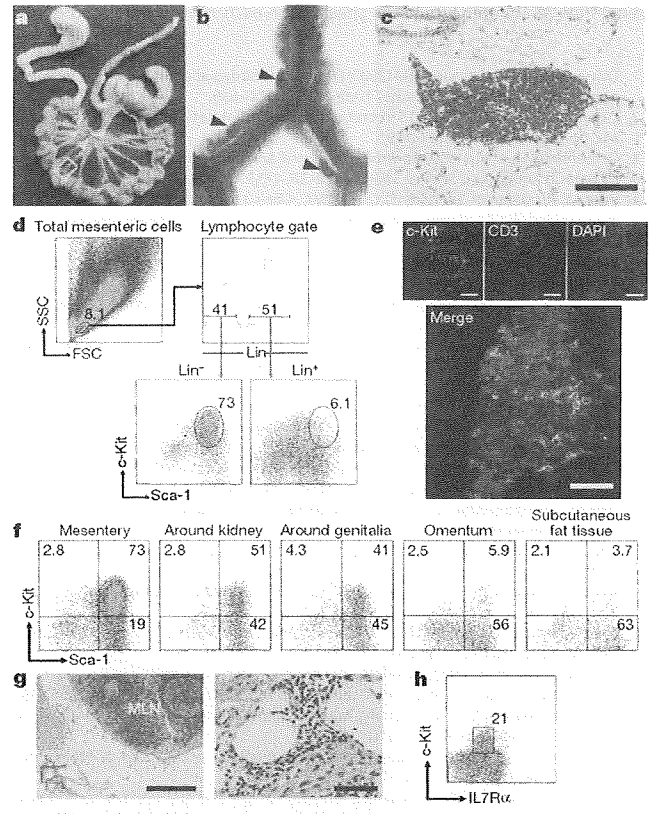

Figure 1 | Lin$^-$c-Kit$^+$Sca-1$^+$ cells exist in FALCs. a, Photograph of mouse mesentery (framed by green line). **b**, A higher magnification of the area framed by the yellow square in **a** after staining with 0.5% toluidine blue. Arrowheads indicate mesenteric lymph nodes (MLN) in **a** and the lymphoid clusters in **b**. **c**, Haematoxylin and eosin (H&E)-stained specimen of a lymphoid cluster in the mesentery. Scale bar, 200 μm. **d**, Flow cytometry of mesenteric cells stained with antibodies against Lin, c-Kit and Sca-1. FSC, forward scatter; SSC, side scatter. **e**, Immunofluorescence staining of a lymphoid cluster. DAPI, 4′,6-diamidino-2-phenylindole. Scale bars, 50 μm. **f**, Flow cytometry of cells isolated from the indicated adipose tissues. **g**, H&E staining of human mesentery. Left: scale bar, 1 mm. Right: a higher magnification photograph of the area framed by the red square in the left panel. Scale bar, 100 μm. **h**, Flow cytometry of human mesenteric cells stained with c-Kit and IL7Rα.

[1]Department of Microbiology and Immunology, [2]Department of Pathology, [3]Department of Tropical Medicine and Parasitology, Keio University School of Medicine, Shinjuku-ku, Tokyo 160-8582, Japan. [4]Japan Science and Technology Agency (JST), CREST, Chiyoda-ku, Tokyo 102-0075, Japan. [5]Laboratory for Lymphocyte Development, Riken Research Center for Allergy and Immunology, Yokohama, Kanagawa 230-0045, Japan. [6]Department of Cell Signalling, Institute of Biomedical Science, Kansai Medical University, Moriguchi, Osaka 570-8506, Japan. [7]Research Center for Science Systems, Japan Society for the Promotion of Science (JSPS), Chiyoda-ku, Tokyo 102-8472, Japan.

made up 20–40% of total lymphocytes in mesenteric cells, comprising 0.5–2 × 10^5 cells per mouse. The clusters contained c-Kit$^+$ cells interspersed with CD3$^+$ T cells and B220$^+$ B cells (Fig. 1e and Supplementary Fig. 2a). Lin$^-$c-Kit$^+$Sca-1$^+$ cells were also found in adipose tissues around the kidney and genitalia, but very few were found in the subcutaneous fat tissue or omentum (Fig. 1f). Hence, we named these lymphoid clusters 'fat-associated lymphoid clusters' or FALCs. The structure of FALCs is similar to that of omental milky spots[12] in that both contain lymphocytes framed by adipose tissue in the peritoneal cavity. However, milky spots contain T- and B-cell zones but few c-Kit$^+$Sca-1$^+$ cells (Fig. 1f and Supplementary Fig. 2). Similar lymphocyte clusters distinct from lymph nodes were found in the human mesentery (Fig. 1g). Human FALCs contained a clearly evident cell population expressing c-Kit and IL7Rα (Fig. 1h).

Giemsa staining showed that FALC c-Kit$^+$Sca-1$^+$ cells were small in size and had a round shape, dark nucleus and scanty cytoplasm (Fig. 2a)—all characteristics of lymphoid cells. Electron microscopy confirmed a high nucleus/cytoplasm ratio and scanty cytoplasm, and also showed a poorly developed Golgi apparatus and endoplasmic reticulum (Fig. 2b). FALC c-Kit$^+$Sca-1$^+$ cells expressed CD45 (encoded by *Ptprc*), IL7Rα, Thy-1.2 (Thy1), CD27, T1/ST2 (IL1RL1, a subunit of IL33R)[13] and activation markers such as CD25 (IL2RA), CD38, CD44, CD69 and GITR (Tnfrsf18) (Fig. 2c). This population was present in *Rag2*$^{-/-}$ and *nu/nu* mice but absent from *gc*$^{-/-}$ (also known as *Il2rg*$^{-/-}$) and *Il7*$^{-/-}$ mice (Fig. 2d), indicating that this population is probably of lymphoid lineage with differentiation dependent on IL7. Culturing FALC c-Kit$^+$Sca-1$^+$ cells on TSt-4/DLL1, a thymic stroma cell line expressing delta-like 1 (DLL1), which supports the development of T-cell progenitors to mature T cells[14], did not induce T-cell differentiation (Supplementary Fig. 3). FALC c-Kit$^+$Sca-1$^+$ cells also did not differentiate into B cells when co-cultured with TSt-4 cells (Supplementary Fig. 3). Furthermore, no differentiation of NK cells or the recently identified NK1.1$^+$NKp46$^+$ cells producing IL22 (ref. 15) was observed either *in vitro* or *in vivo* (data not shown). FALC c-Kit$^+$Sca-1$^+$ cells are also phenotypically similar to LTi cells[4]. As shown in Fig. 2d, γ_c and Id2 (ref. 16), critical for the differentiation of LTi cells, are also required for the development of FALC c-Kit$^+$Sca-1$^+$ cells. However, this population was present in *Rorc*$^{GFP/GFP}$ mice, which lack LTi cells[17]. FALCs were also present in *aly/aly* mice (Supplementary Fig. 4) but *Rorc*$^{GFP/GFP}$ and *aly/aly* mice have reduced percentages of c-Kit$^+$Sca-1$^+$ cells (Fig. 2d). Mutations in SCF (*Sl/Sl*^{d}) and c-Kit (*W/W*^{v}) resulted in the reduction of c-Kit$^+$Sca-1$^+$T1/ST2$^+$ cells (Fig. 2e), suggesting that the SCF/c-Kit pathway is in part involved in the differentiation of FALC c-Kit$^+$Sca-1$^+$ cells.

The gene expression pattern of sorted FALC c-Kit$^+$Sca-1$^+$ cells examined by microarray analysis differed from those of thymic DN2 and LTi cells (Supplementary Fig. 5). *Tnfrsf11a* (encoding RANK) and *Rorc* (encoding RORγ) were expressed in LTi cells but not in FALC c-Kit$^+$Sca-1$^+$ cells (Supplementary Fig. 5). Semi-quantitative PCR with reverse transcription (RT–PCR) analysis supported these differences (Fig. 2f). The lack of RORγ expression also indicates that these cells are distinct from IL22-producing NKp46$^+$ cells, which express a high amount of RORγ[15]. T1/ST2 was highly expressed on FALC c-Kit$^+$Sca-1$^+$ cells (Fig. 2c) but not on DN2 or LTi cells (data not shown). These results collectively indicate that FALC c-Kit$^+$Sca-1$^+$ cells belong to a new lymphocyte lineage characterized by the expression of c-Kit, IL7R and IL33R. FALC c-Kit$^+$Sca-1$^+$ cells expressed several T_H2 cytokines including IL4, IL5, IL6 and IL13 (Fig. 2g). Consistently, the expression of T_H2-related genes such as *Maf* (c-Maf), *Gata3* (Gata3), *Junb* (JunB) and *Stat6* (Stat6) were readily detected in FALC c-Kit$^+$Sca-1$^+$ cells (Fig. 2h).

Among the cytokines tested—including Flt3l, SCF (also known as Kitl), IL1β, IL2, IL3, IL4, IL5, IL6, IL7, IL9, IL15, IL25, IL33, M-CSF (Csf1), GM-CSF (Csf2), TNFα and TGFβ1—we found that SCF and IL7 supported the survival of FALC c-Kit$^+$Sca-1$^+$ cells (Fig. 3a and data not shown), as expected by their expression of c-Kit and IL7Rα. These cells survived for several weeks on TSt-4 feeder cells (Supplementary Fig. 3) and proliferated in response to IL2 for an extended time period (up to 42 days) without changing surface phenotype (Fig. 3a and Supplementary Fig. 6), raising the possibility that these cells are terminally differentiated effector cells. ELISA analyses showed that FALC c-Kit$^+$Sca-1$^+$ cells are indeed capable of producing large amounts of IL2, IL4, IL5, IL6, GM-CSF and a moderate amount of IFNγ in response to phorbol myristate acetate (PMA) plus ionomycin (Fig. 3b). The amounts of T_H2 cytokines produced by FALC c-Kit$^+$Sca-1$^+$ cells (Fig. 3b, filled bars) were substantially higher than those produced by CD4$^+$ T cells from spleen (Fig. 3b, open bars) or mesenteric lymph nodes (MLN) (Fig. 3b, grey bars). IL5 and IL6 were detected even in the culture with IL7 alone, and IL2 increased the production of these cytokines. Concanavalin A and LPS (lipopolysaccharide) had no effect on cytokine production. Notably, IL33 and a combination of IL2 and IL25 induced extremely high amounts of IL5 and IL13 (microgram amounts from 5,000 cells) but little IFNγ (Fig. 3c, d). IL33 did not induce IL17 production. Basophils and mast cells also express T1/ST2 and produce IL13 in response to IL33 (refs 18, 19),

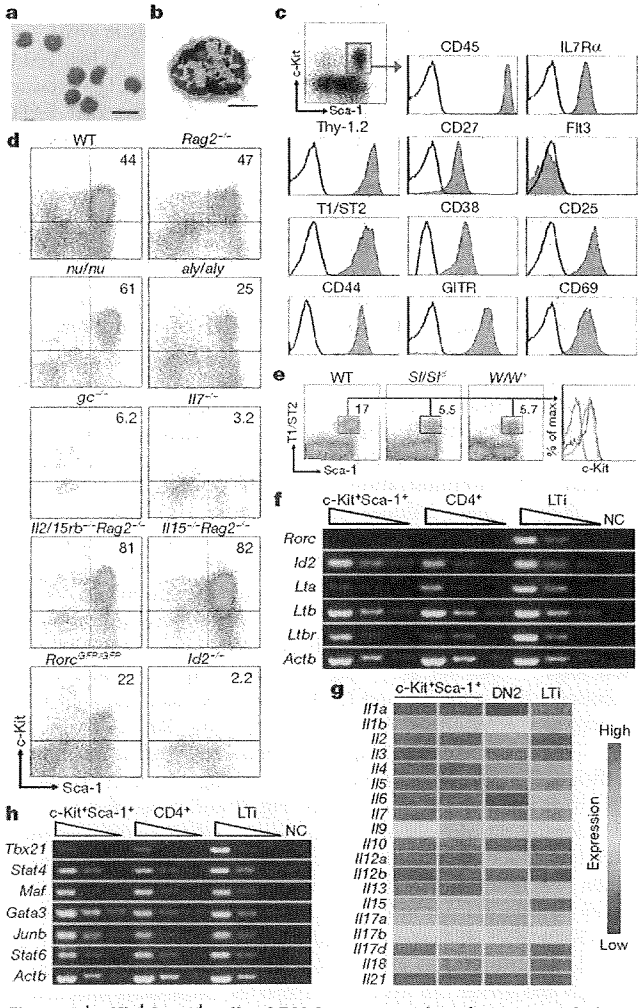

Figure 2 | c-Kit$^+$Sca-1$^+$ cells of FALCs are a new lymphocyte population. **a**, **b**, Giemsa staining (**a**) and electron micrograph (**b**) of sorted FALC c-Kit$^+$Sca-1$^+$ cells. Scale bars, 20 μm (**a**) and 2 μm (**b**). **c**, Flow cytometry of FALC c-Kit$^+$Sca-1$^+$ cells. **d**, **e**, Flow cytometry of mesenteric cells from the indicated strains of mice. Numbers indicate the percentages of c-Kit$^+$Sca-1$^+$ (**d**) and Sca-1$^+$T1/ST2$^+$ (**e**) cells. Histograms in **e** show the expression levels of c-Kit on wild-type (green), *Sl/Sl*^{d} (blue) and *W/W*^{v} (red) Sca-1$^+$T1/ST2$^+$ cells. **f**, **h**, Semi-quantitative RT–PCR analysis of the indicated genes. NC, negative control (no template). **g**, Microarray analysis of cytokine gene expression of FALC c-Kit$^+$Sca-1$^+$ (in duplicate), DN2 and LTi cells.